

AdaSCALE: Adaptive Scaling for OOD Detection

Sudarshan Regmi

sudarshanregmi9@gmail.com

Abstract

The ability of the deep learning model to recognize when a sample falls outside its learned distribution is critical for safe and reliable deployment. Recent state-of-the-art out-of-distribution (OOD) detection methods leverage activation shaping to improve the separation between in-distribution (ID) and OOD inputs. These approaches resort to sample-specific scaling but apply a static percentile threshold across all samples regardless of their nature, resulting in suboptimal ID-OOD separability. In this work, we propose **AdaSCALE**, an adaptive scaling procedure that dynamically adjusts the percentile threshold based on a sample’s estimated OOD likelihood. This estimation leverages our key observation: OOD samples exhibit significantly more pronounced activation shifts at high-magnitude activations under minor perturbation compared to ID samples. AdaSCALE enables stronger scaling for likely ID samples and weaker scaling for likely OOD samples, yielding highly separable energy scores. Our approach achieves state-of-the-art OOD detection performance, outperforming the latest rival OptFS by **14.94%** in near-OOD and **21.67%** in far-OOD datasets in average FPR@95 metric on the ImageNet-1k benchmark across eight diverse architectures. The code is available at: <https://github.com/sudarshanregmi/AdaSCALE/>

1. Introduction

The reliable deployment of deep learning models hinges on their ability to handle previously unseen inputs, a task commonly known as OOD detection. One critical application is in medical diagnosis, where a model trained on common diseases should be able to flag inputs representing unknown conditions as potential outliers, requiring further review by clinicians. OOD detection primarily involves identifying semantic shifts, with robustness to covariate shifts being a highly desirable characteristic [2, 58]. As modern deep learning models scale in both data and parameter counts, effective OOD detection within large-scale settings is critical. Given the difficulties of iterating on large models, *post-hoc* approaches that preserve ID accuracy are generally preferred.

A variety of post-hoc approaches have emerged, broadly

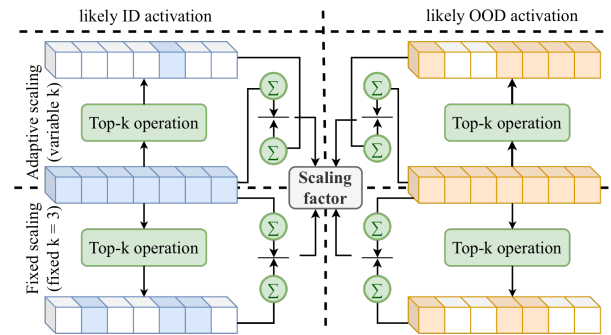


Figure 1. **Adaptive scaling (AdaSCALE) vs. fixed scaling (ASH [7], SCALE [54], LTS [8]).** While fixed scaling approaches uses a constant percentile threshold p and hence constant k (e.g., $k = 3$) across all samples, AdaSCALE adjusts k based on estimated OOD likelihood. AdaSCALE assigns larger k values (e.g., $k = 5$) to OOD-likely samples, producing smaller scaling factors, and smaller k values (e.g., $k = 1$) to ID-likely samples, yielding larger scaling factors. This adaptive mechanism enhances ID-OOD separability. (See Figure 2 for complete working mechanism.)

categorized by where they operate. One class of methods focuses on computing OOD scores directly in the output space [7, 16, 20, 30, 33, 64], while another operates in the activation space [27, 40, 44, 48]. Finally, a more recent line of research also explores a hybrid approach [24, 50], combining information from both spaces. The efficacy of many high-performing methods relies on either accurate computation of ID statistics [25, 26, 46, 47, 55] or retention of training data statistics [40, 48]. However, as retaining full access to training data becomes increasingly impractical in large-scale settings, methods that operate effectively with minimal ID samples without performance degradation are particularly valuable for practical applications.

Alleviating the dependence on ID training data/statistics, recent state-of-the-art post-hoc approaches center around the concept of “fixed scaling.” ASH [7] prunes and scales activations on a per-sample basis. SCALE [54], the direct successor of ASH, critiques pruning and focuses purely on scaling, which improves OOD detection without accuracy

degradation. LTS [8] extends this concept by directly scaling logits instead, using post-ReLU activations. These methods leverage a key insight: scaling based on the relative strength of a sample’s *top-k* activations (with respect to the entire activations) produces highly separable ID-OOD energy scores. However, although such approaches provide sample-specific scaling factors, the scaling mechanism remains uniform across all samples as the percentile threshold p and thereby k is fixed, as shown in Figure 1. This static approach is inherently limiting for optimal ID-OOD separation while also failing to leverage even minimal ID data, which could be reasonably practical in most deployment scenarios.

We hypothesize that designing an adaptive scaling procedure based on each sample’s predetermined OOD likelihood offers greater control for enhancing ID-OOD separability. Specifically, this mechanism should assign smaller scaling factors for samples with high OOD likelihood to yield lower energy scores and larger scaling factors for probable ID samples to yield higher energy scores. To achieve this, we propose a heuristic for predetermining OOD likelihood based on a key observation in activation space: minor perturbations applied to OOD samples induce significantly more pronounced shifts in their top-k activations compared to ID samples. Consequently, samples exhibiting substantial activation shifts are assigned lower scaling factors, while those with minimal shifts receive higher scaling factors. This adaptive scaling mechanism can be applied in either logit or activation space. Our method, **AdaSCALE**, achieves state-of-the-art performance, delivering significant improvements in OOD detection while requiring only minimal ID samples.

We conduct an extensive evaluation across 8 architectures on ImageNet-1k and 2 architectures on CIFAR benchmarks, demonstrating the substantial effectiveness of AdaSCALE. For instance, AdaSCALE surpasses the average performance of the *best-generalizing* method, OptFS [64], by **14.94%/8.96%** for near-OOD detection and **21.48%/3.39%** for far-OOD detection in terms of FPR@95 / AUROC, on the ImageNet-1k benchmark across eight architectures. Furthermore, AdaSCALE outperforms the *best-performing* method, SCALE [54], when evaluated on the ResNet-50 architecture, achieving performance gains of **12.95%/6.44%** for near-OOD and **16.79%/0.79%** for far-OOD detection. Additionally, AdaSCALE consistently demonstrates superiority in full-spectrum OOD detection [58]. Our key contributions are summarized as follows:

- We reveal that OOD inputs exhibit significantly more pronounced shifts in top-k activations under minor perturbations compared to ID inputs.
- Leveraging this observation, we propose a novel post-hoc OOD detection method utilizing adaptive scaling that attains state-of-the-art OOD detection.
- We demonstrate state-of-the-art generalization of AdaSCALE via extensive evaluations across many setups.

2. Related Works

Post-hoc methods. Early research on OOD detection primarily focused on designing scoring functions based on logit information [16, 20, 30, 33, 34]. While these methods leveraged logit-based scores, alternative approaches have explored gradient-based information, such as GradNorm [23], GradOrth [4], GAIA [5], and Greg-OOD [45]. Given the limited dimensionality of the logit space, which may not encapsulate sufficient information for OOD detection, subsequent studies have investigated activation-space-based methods. These approaches exploit the high-dimensional activations, leading to both parametric techniques such as MDS [27], MDS Ensemble [27], and RMDS [44], as well as non-parametric methods such as KNN-based OOD detection [39, 48]. Recent advancements have proposed hybrid methodologies that integrate parametric and non-parametric techniques to improve robustness. For instance, ComboOOD [40] combines these paradigms to enhance near-OOD detection performance. Similarly, VIM [50] employs a combination of logit-based and distance-based metrics. However, reliance of such approaches on ID statistics [38, 46, 59] can become a constraint, hindering scalability and practical deployment in real-world applications. To mitigate computational challenges for real-world deployment, recent methods, such as FDBD [32] and NCI [31], have focused on enhancing efficiency. Recent advances, such as WeiPer [14], explore class-direction perturbations, while NECO [1] examines connections to neural collapse phenomena.

Activation-shaping post-hoc methods. A seminal work in OOD detection, ReAct [47], identified abnormally high activation patterns in OOD samples and proposed clipping extreme activations. This approach has been further generalized by BFAct [25] and VRA [55], which extend activation clipping for enhanced effectiveness. Additionally, BATS [66] refines activation distributions by aligning them with their respective typical sets, while LAPS [15] enhances this strategy by incorporating channel-aware typical sets. Inspired by activation clipping, another line of research explores activation “scaling” as a means to improve OOD detection. ASH [7] introduces a method to compute a scaling factor as a function of the activation itself, pruning and rescaling activations to enhance the separation of energy scores between ID and OOD samples. However, this approach results in a slight degradation in ID classification accuracy. In response, SCALE [54] observes that pruning adversely affects performance and thus eliminates it, leading to improved OOD detection while preserving ID accuracy. SCALE currently represents the state-of-the-art method for ResNet-50-based OOD detection. Despite their efficacy, these activation-based methods exhibit limited generalization across diverse architectures. To address this issue,

LTS [8] extends SCALE by computing scaling factors using post-ReLU activations and applying them directly to logits rather than activations. Our work builds on this line of work, introducing the adaptive scaling mechanism. ATS [26] argues that relying solely on final-layer activations may result in the loss of critical information beneficial for OOD detection and proposes to leverage intermediate-layer activations too. However, its efficacy is contingent upon the availability of a large number of training samples, whereas our approach attains state-of-the-art performance while utilizing a minimal number of ID samples. A newly proposed method OptFS [64] introduces a piecewise constant shaping function with the goal of generalization across diverse architectures in large-scale settings, while our work exhibits superior generalization extending to small-scale settings too.

Training methods. The training methods incorporate adjustments during training to enhance the ID-OOO differentiating characteristics. They either make architectural adjustments [6, 18, 22], apply enhanced data augmentations [19, 21, 53], or make simple training modifications [42, 52, 62]. More recent methods have adopted contrastive learning in the context of OOD detection [35, 36, 43, 67]. Moreover, some approaches also either utilize external real outliers [11, 17, 60, 65] or synthesize virtual outliers either in image space [3, 10, 13, 29, 37, 41, 51, 63] or in feature space [9, 12, 28, 49]. However, training strategies incur additional computational cost and potentially inferior performance to post-hoc methods in large-scale setups [57].

3. Preliminaries

Let \mathcal{X} denote the input space and $\mathcal{Y} = \{1, 2, \dots, C\}$ denote the label space, where C is the number of classes. We consider a multi-class classification setting where a classifier h is trained on ID data drawn from an underlying joint distribution $\mathcal{P}_{\text{ID}}(x, y)$, where $x \in \mathcal{X}$ and $y \in \mathcal{Y}$. The ID training dataset is denoted as $\mathcal{D}_{\text{ID}} = \{(x_i, y_i)\}_{i=1}^N$, where N is the number of training samples and $(x_i, y_i) \sim \mathcal{P}_{\text{ID}}(x, y)$.

The classifier h is composed of a feature extractor $f_\theta : \mathcal{X} \rightarrow \mathcal{A} \in \mathbb{R}^D$, and a classifier $g_W : \mathcal{A} \rightarrow \mathcal{Z} \in \mathbb{R}^C$. The feature extractor maps an input x to a feature vector $\mathbf{a} \in \mathcal{A}$, where $\mathbf{a} = f_\theta(x)$ and the classifier then maps this feature vector to a logit vector $\mathbf{z} = g_W(\mathbf{a}) \in \mathbb{R}^C$. We refer to individual dimensions of the feature vector \mathbf{a} as activations, denoted by a_j for the j -th dimension. The classifier h is trained on \mathcal{D}_{ID} to minimize the empirical risk:

$$\min_{\theta, W} \frac{1}{N} \sum_{i=1}^N \mathcal{L}(g_W(f_\theta(x_i)), y_i) \quad (1)$$

where \mathcal{L} is a loss function, such as cross-entropy loss. During inference, the model may encounter data points drawn from a different distribution, denoted as $\mathcal{P}_{\text{OOD}}(x)$, which is

referred to as OOD data. The OOD detection problem aims to identify whether a given input x is drawn from marginal distribution $\mathcal{P}_{\text{ID}}(x)$ or from $\mathcal{P}_{\text{OOD}}(x)$. Hence, the goal is to design a scoring function $S(x) : \mathcal{X} \rightarrow \mathbb{R}$ that assigns a scalar score to each input x , reflecting its likelihood of being an OOD sample. A higher score typically indicates a higher probability of the input being OOD. A threshold τ is used to classify an input as either ID or OOD:

$$\text{OOD}(x) = \begin{cases} \text{True}, & \text{if } S(x) > \tau \\ \text{False}, & \text{if } S(x) \leq \tau \end{cases} \quad (2)$$

4. Method

In this section, we introduce AdaSCALE, a novel post-processing approach that dynamically adapts the scaling mechanism based on each sample’s estimated OOD likelihood. We first present our key empirical observations regarding activation behavior under minor perturbations, building upon insights from ReAct [47]. Next, we revisit and analyze the core principle underlying recent state-of-the-art approaches. Finally, we detail our proposed adaptive scaling mechanism that leverages these observations to achieve superior OOD detection performance.

4.1. Observations in Activation Space

A seminal work ReAct [47] demonstrated that OOD samples often induce abnormally high activations within neural networks. We extend this finding with an important observation: *the positions of such high activations in OOD samples are relatively unstable under minor perturbations compared to ID samples*. This instability provides a valuable signal for distinguishing OOD samples from ID samples. Below, we formalize this observation and our methodology.

4.1.1. Perturbation Mechanism

Let $x \in \mathbb{R}^{C_{\text{in}} \times H \times W}$ be an input image with C_{in} input channels, H height, and W width. We denote channel value at position (c, h, w) as $x[c, h, w]$. To identify channel values for perturbation, we employ pixel attribution that quantifies each input element’s influence on the model’s prediction. An attribution function, $AT(x, c, h, w)$, assigns a score to each channel value, with *lower* absolute scores indicating *less* influence. We select $o\%$ of channel value indices with *lowest* absolute attribution scores, forming the set R . We use a gradient-based attribution:

$$AT(x, c, h, w) = \frac{\partial (g_W(f_\theta(x)))_{y_{\text{pred}}}}{\partial x[c, h, w]} \quad (3)$$

where y_{pred} is the predicted class index. To create a perturbed input, we select a subset R containing $o\%$ of channel

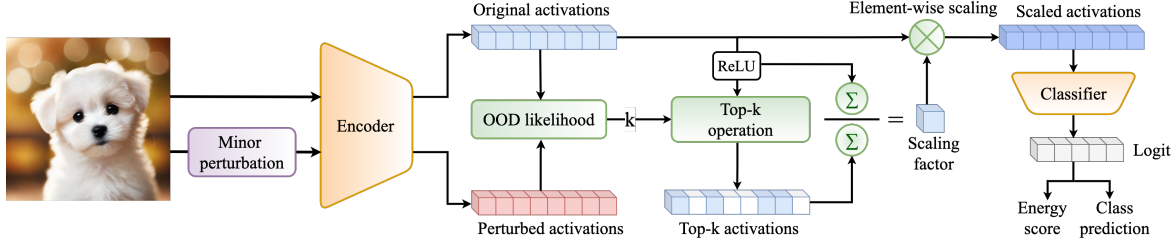


Figure 2. **Schematic diagram of AdaSCALE’s working mechanism.** AdaSCALE computes activation shifts between an original image and its slightly perturbed counterpart to estimate OOD likelihood. This likelihood determines an adaptive percentile threshold (p and thereby k), which controls the scaling factor r . Since r is defined as the ratio of total activation sum to the sum of activations above the percentile threshold, samples with higher OOD likelihood receive lower scaling factors. This adaptive approach ensures stronger scaling for ID samples and weaker scaling for OOD samples, yielding highly separable energy scores that enable effective OOD detection.

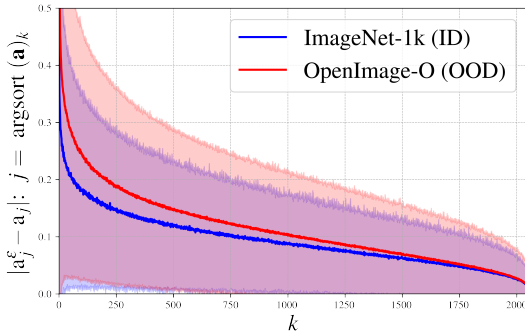


Figure 3. Activation shift comparison (with the mean denoted by a solid line and the standard deviation by a shaded region) between ID and OOD in the ResNet-50 model. The activation shift is significantly more pronounced in OOD samples compared to ID samples at high-magnitude activations (left side of the x-axis), providing a discriminative signal for OOD detection.

values to perturb. The perturbed image x^ε is obtained as:

$$x^\varepsilon[c, h, w] = \begin{cases} x[c, h, w] + \varepsilon \cdot \text{sign}(AT(x, c, h, w)), & \text{if } (c, h, w) \in R \\ x[c, h, w], & \text{if } (c, h, w) \notin R \end{cases} \quad (4)$$

where ε is perturbation magnitude.

4.1.2. Activation Shift as OOD Indicator

After obtaining the perturbed input x^ε , we compute its activation $\mathbf{a}^\varepsilon = f_\theta(x^\varepsilon)$. We define the *activation shift* as the absolute element-wise difference between the original activation and the perturbed activation:

$$\mathbf{a}^{\text{shift}} = |\mathbf{a}^\varepsilon - \mathbf{a}| \quad (5)$$

Figure 3 illustrates the key insight of our approach: activation shift at extreme (high-magnitude) activations is consistently more pronounced in OOD samples compared to ID samples. This behavior can be understood intuitively: ID samples activate network features in a stable, predictable manner reflecting learned patterns, while OOD samples trigger less stable, more arbitrary high activations that shift

significantly under perturbation. Based on this observation, we propose using activation shift at the top- k_1 highest activations as a metric to estimate OOD likelihood of a sample:

$$Q = \sum_{j \in \text{argsort}(\mathbf{a}, \text{desc}=\text{True})[:k_1]} (|a_j^\varepsilon - a_j|) \quad (6)$$

where $\text{argsort}(\mathbf{a}, \text{desc}=\text{True})[:k_1]$ returns the indices of the k_1 highest values in \mathbf{a} . As evidenced by $Q_{\text{OOD}}/Q_{\text{ID}}$ ratio shown in Figure 4, the Q statistic generally assigns higher values to diverse OOD samples than ID samples. However, the high variance of Q metric (Figure 3) suggests the possibility of overoptimistic estimations. To address this issue, we introduce a correction term C_o that exhibits an opposing behavior: it tends to be higher for ID samples than for OOD samples. Figure 5 shows that the perturbed activations of ID samples tend to be higher than those of OOD samples, especially in high-activation regions. We leverage this complementary signal by defining:

$$C_o = \sum_{j \in \text{argsort}(\mathbf{a}, \text{desc}=\text{True})[:k_2]} \text{ReLU}(a_j^\varepsilon) \quad (7)$$

where k_2 is a hyperparameter denoting the number of considered activations. We refine our OOD quantification by combining both metrics, weighted by a hyperparameter λ :

$$Q' = \lambda \cdot Q + C_o \quad (8)$$

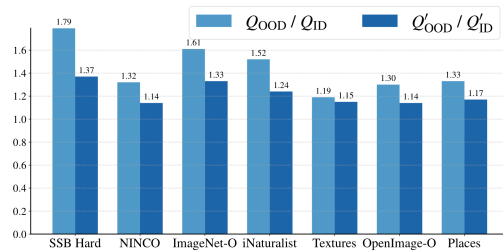


Figure 4. $Q_{\text{OOD}} / Q_{\text{ID}}$ vs $Q'_{\text{OOD}} / Q'_{\text{ID}}$ across various OOD datasets with ResNet-50 model trained in ImageNet-1k.

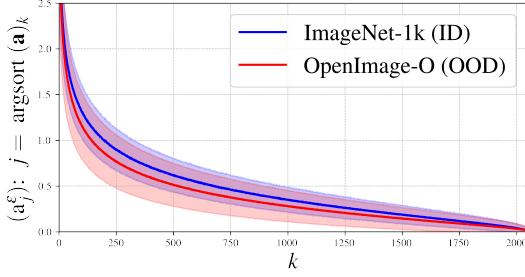


Figure 5. Perturbed activation magnitudes comparison between ID and OOD samples. ID samples consistently maintain higher average activation values in comparison to OOD samples.

If $\bar{Q}_s = \{\bar{Q}'_1, \bar{Q}'_2, \dots, \bar{Q}'_{n_{\text{val}}}\}$ be the set of Q' values on n_{val} ID validation samples, we could transform any Q' into a normalized probability scale by constructing empirical cumulative distribution function (eCDF) derived from \bar{Q}_s . The eCDF, denoted as $F_{Q'}(Q')$, can be defined as:

$$F_{Q'}(Q') = \frac{1}{n_{\text{val}}} \sum_{i=1}^{n_{\text{val}}} \mathbb{1}(\bar{Q}'_i \leq Q') \quad (9)$$

where $\mathbb{1}(\cdot)$ is the indicator function. A higher value of $F_{Q'}(Q')$ indicates a higher likelihood of the sample being OOD. Importantly, our experiments suggest that as few as 10 ID validation samples are sufficient to construct an effective eCDF for this purpose (See Table 7).

4.2. Revisiting Static Scaling Mechanisms

Recent state-of-the-art post-processing methods for OOD detection, including SCALE [54], ASH [7], and LTS [8], operate by scaling either the activations or logits. The scaling factor r is computed as:

$$r = \left(\frac{\sum_j \mathbf{a}_j}{\sum_{\mathbf{a}_j > P_p(\mathbf{a})} \mathbf{a}_j} \right) \quad (10)$$

where $P_p(\mathbf{a})$ denotes the p^{th} percentile of all elements in activation \mathbf{a} . While this approach yields sample-specific scaling factors, it imposes a critical constraint: the p^{th} percentile threshold is static and identical across all test samples, regardless of the nature of samples. We argue that this static nature limits the effectiveness of the scaling procedure and prevents optimal ID-OOD separability.

4.3. Proposed Approach: Adaptive Scaling

Building on our observations, we propose AdaSCALE (Adaptive SCALE), a novel approach that introduces dynamic, sample-specific adjustments to the scaling procedure. The key insight of AdaSCALE is that the p^{th} percentile threshold should be a function of each test sample's estimated OOD likelihood rather than a fixed value. The scaling

Algorithm 1 Computing the Adaptive Scaling Factor

- 1: **Input:** Input sample x , perturbation magnitude ε , model f_θ , hyperparameters $\lambda, k_1, k_2, p_{\min}, p_{\max}, \varepsilon, o$, pre-computed empirical CDF $F_{Q'}$
 - 2: **Output:** Scaling factor r
 - 3: // Extract features and compute activation shifts
 - 4: $\mathbf{a} \leftarrow f_\theta(x)$ {Original activation}
 - 5: $\nabla_x z_c \leftarrow \frac{\partial gw(f_\theta(x))_c}{\partial x}$ {Gradient for predicted class c }
 - 6: $R \leftarrow o\%$ of channel values with *lowest* $|\nabla_x z_c|$
 - 7: $x^\varepsilon \leftarrow x + \varepsilon \cdot \text{sign}(\nabla_x z_c) \cdot \mathbb{1}_R$ {Perturb selected regions}
 - 8: $\mathbf{a}^\varepsilon \leftarrow f_\theta(x^\varepsilon)$ {Perturbed activation}
 - 9: $\mathbf{a}^{\text{shift}} \leftarrow |\mathbf{a}^\varepsilon - \mathbf{a}|$ {Compute activation shift}
 - 10: // Compute OOD likelihood estimate
 - 11: $\mathbf{i}_1 \leftarrow \text{argsort}(\mathbf{a}, \text{desc} = \text{True})[:k_1]$
 - 12: $Q \leftarrow \sum_{i \in \mathbf{i}_1} a_i^{\text{shift}}$ {Shift in top activations}
 - 13: $\mathbf{i}_2 \leftarrow \text{argsort}(\mathbf{a}, \text{desc} = \text{True})[:k_2]$
 - 14: $C_o \leftarrow \sum_{i \in \mathbf{i}_2} \text{ReLU}(a_i^\varepsilon)$ {Correction term}
 - 15: $Q' \leftarrow \lambda \cdot Q + C_o$ {OOD likelihood estimate}
 - 16: // Compute adaptive percentile
 - 17: $p_r \leftarrow (1 - F_{Q'}(Q'))$ {raw ID likelihood from eCDF}
 - 18: $p \leftarrow p_{\min} + p_r \cdot (p_{\max} - p_{\min})$ {Adjusted percentile}
 - 19: // Compute scaling factor
 - 20: $P_p(\mathbf{a}) \leftarrow$ the p -th percentile value of all elements in \mathbf{a}
 - 21: $r \leftarrow \sum_j a_j / \sum_{a_j > P_p(\mathbf{a})} a_j$ {Final scaling factor}
 - 22: **return** r
-

factor r increases as the p^{th} percentile threshold rises (i.e., when more activations are excluded from the denominator in Equation 10). For optimal ID-OOD separation, we must scale ID samples more strongly than OOD samples, requiring a higher p^{th} percentile for ID samples. Leveraging Q' as an OOD likelihood estimator, we can now define an adaptive percentile threshold as:

$$p = p_{\min} + \left(1 - F_{Q'}(Q')\right) \cdot (p_{\max} - p_{\min}) \quad (11)$$

where p_{\min} and p_{\max} are hyperparameters that define the minimum and maximum limits of percentile threshold. It ensures that samples with lower OOD likelihood (i.e., likely ID samples) receive higher percentile thresholds, resulting in stronger scaling. Algorithm 1 summarizes our adaptive scaling factor computation procedure. We implement two variants: **AdaSCALE-A** scales activations as $\mathbf{a}_{\text{scaled}} = \mathbf{a} \cdot \exp(r)$, similar to ASH [7] and SCALE [54]. **AdaSCALE-L** scales logits as $\mathbf{z}_{\text{scaled}} = \mathbf{z} \cdot r^2$, similar to LTS [8]. For OOD detection, we use the energy score $-\log \sum_{i=1}^C e^{(\mathbf{z}_i)}$ on (directly or indirectly) scaled logits, with higher values indicating higher ID likelihood. This approach enables per-sample dynamic scaling, as outlined in Figure 2.

Method	ResNet-50	ResNet-101	RegNet-Y-16	ResNeXt-50	DenseNet-201	EfficientNetV2-L	ViT-B-16	Swin-B	Average	
near-OOD	MSP	74.23 / 60.21	71.96 / 67.25	62.22 / 80.74	73.25 / 67.86	73.44 / 67.29	72.51 / 80.76	86.72 / 68.62	87.11 / 69.82	75.18 / 70.32
	MLS	74.87 / 64.55	72.05 / 71.51	62.94 / 84.66	74.11 / 71.62	75.51 / 68.91	81.44 / 79.22	93.78 / 63.64	94.80 / 64.68	78.69 / 71.10
	EBO	75.32 / 64.52	72.32 / 71.54	62.80 / 84.76	74.21 / 71.61	75.85 / 68.68	82.86 / 77.15	94.37 / 59.19	95.34 / 59.79	79.13 / 69.66
	ReAct	72.61 / 68.81	68.07 / 75.00	70.73 / 75.37	70.96 / 74.13	69.97 / 73.65	72.36 / 71.39	86.63 / 68.35	82.64 / 73.26	74.25 / 72.50
	ASH	69.47 / 71.33	65.24 / 76.61	82.51 / 67.81	70.98 / 75.25	92.83 / 52.30	94.85 / 44.78	94.45 / 53.20	96.37 / 47.58	83.34 / 61.11
	SCALE	67.76 / 74.20	63.87 / 78.60	67.09 / 82.90	70.59 / 76.20	71.56 / 73.72	89.70 / 60.12	94.48 / 56.18	88.62 / 61.47	76.71 / 70.42
	BFAct	72.35 / 68.88	67.96 / 75.16	78.72 / 66.09	70.96 / 74.14	71.20 / 72.61	75.53 / 62.46	82.09 / 70.66	71.81 / 75.28	73.83 / 70.66
	LTS	68.01 / 73.37	63.91 / 78.27	69.82 / 80.75	70.27 / 76.20	71.29 / 74.56	87.30 / 73.63	88.83 / 67.43	86.61 / 67.22	75.76 / 73.93
	OptFS	69.66 / 70.97	65.46 / 75.83	73.53 / 75.21	69.27 / 74.84	71.74 / 72.10	72.29 / 75.29	76.55 / 72.73	76.81 / 74.06	71.91 / 73.88
	AdaSCALE-A	58.98 / 78.98	<u>57.96 / 81.68</u>	47.91 / 89.18	<u>64.14 / 79.96</u>	61.28 / 79.66	53.78 / 86.94	71.87 / 73.14	73.41 / 74.48	61.17 / 80.50
AdaSCALE-L	<u>59.84 / 78.62</u>	56.41 / 81.86	<u>56.13 / 87.11</u>	62.08 / 80.18	<u>61.75 / 80.06</u>	<u>54.95 / 85.77</u>	<u>71.99 / 73.23</u>	<u>72.89 / 74.58</u>	<u>62.00 / 80.18</u>	
far-OOD	MSP	53.15 / 84.06	53.87 / 83.81	40.41 / 90.08	53.07 / 84.21	53.60 / 84.43	54.74 / 87.92	56.41 / 84.62	73.39 / 82.02	54.83 / 85.14
	MLS	42.57 / 88.19	43.89 / 88.30	32.92 / 93.70	44.91 / 87.97	48.43 / 87.44	68.64 / 84.80	81.89 / 81.42	95.16 / 73.37	57.30 / 85.65
	EBO	42.72 / 88.09	44.30 / 88.23	32.47 / 93.82	45.12 / 87.86	48.95 / 87.15	74.48 / 81.13	86.95 / 76.34	96.08 / 63.99	58.88 / 83.33
	ReAct	30.14 / 92.98	29.89 / 93.10	45.20 / 86.17	30.06 / 92.69	30.72 / 92.65	60.05 / 75.33	59.31 / 83.65	58.86 / 84.77	43.03 / 87.67
	ASH	24.69 / 94.43	26.18 / 94.06	59.65 / 83.94	29.17 / 93.47	33.50 / 92.17	96.56 / 41.57	95.98 / 52.16	98.23 / 43.20	57.99 / 74.38
	SCALE	21.44 / 95.39	22.54 / 95.05	32.16 / 94.16	30.62 / 93.54	33.17 / 92.70	89.63 / 62.58	88.36 / 72.32	86.59 / 66.77	50.56 / 84.06
	BFAct	29.46 / 93.01	29.43 / 93.04	58.69 / 77.22	29.71 / 92.67	32.45 / 92.29	66.72 / 65.70	51.58 / 85.77	38.99 / 88.47	42.13 / 86.02
	LTS	22.20 / 95.24	23.07 / 94.94	34.99 / 93.57	30.37 / 93.49	30.92 / 93.29	86.85 / 76.30	64.37 / 84.43	85.84 / 44.80	47.33 / 84.51
	OptFS	25.66 / 93.87	26.97 / 93.55	47.37 / 86.73	27.54 / 93.40	34.42 / 91.04	53.62 / 83.62	46.11 / 87.35	<u>44.27 / 87.79</u>	38.25 / 89.67
	AdaSCALE-A	17.84 / 96.14	18.51 / 95.95	<u>21.37 / 95.84</u>	22.08 / 95.24	<u>28.01 / 93.23</u>	37.61 / 91.48	47.63 / 86.83	47.81 / 87.14	<u>30.11 / 92.73</u>
AdaSCALE-L	<u>17.92 / 96.12</u>	<u>19.15 / 95.76</u>	20.10 / 96.19	<u>22.16 / 95.01</u>	28.00 / 93.18	<u>38.81 / 90.51</u>	<u>47.28 / 86.97</u>	<u>46.24 / 87.97</u>	29.96 / 92.71	

Table 1. OOD detection results (FPR@95 ↓ / AUROC ↑) on ImageNet-1k benchmark across various architectures.

5. Experiments

We use pre-trained models provided by PyTorch for ImageNet-1k experiments. For CIFAR experiments, we train three models per network using the standard cross-entropy loss and report the mean results across these three independent trials. The evaluation setup is provided in Table 2.

Metrics. We use two commonly used OOD Detection metrics: Area Under Receiver-Operator Characteristics (AUROC) and False Positive Rate at 95% True Positive Rate (FPR@95), where a higher AUROC and lower FPR@95 indicates better OOD detection performance.

Baselines. We consider the following post-hoc methods: MSP [16], ODIN [30], EBO [33], ReAct [47], MLS [20], ASH [7], SCALE [54], BFAct [25], LTS [8], OptFS [64]. Currently, SCALE is the *best-performing* method (with ResNet-50), while OptFS is the *best-generalizing* method.

Hyperparameters. The hyperparameters are determined via automatic parameter search provided by OpenOOD [57, 61]. The best results are **bold**, and the second-best results are underlined across all results. We refer readers to Appendices A, B, C D, and E for complete details and studies.

Conventional OOD detection			
ID datasets	Near-OOD	Far-OOD	Network
CIFAR-10/100	CIFAR-100/10 TIN	MNIST, SVHN, Textures, Places365	WRN-28-10, DenseNet-101
ImageNet-1k	SSB-Hard NINCO ImageNet-O	iNaturalist, Places, OpenImage-O Textures Places	EfficientNetV2-L, ResNet-101 DenseNet-201, ViT-B-16 ResNet-50, ResNeXt-50 RegNet-Y-16, Swin-B
Covariate shifted datasets for full spectrum OOD detection			
ImageNet-1k	ImageNet-C, ImageNet-R, ImageNet-V2, ImageNet-ES		

Table 2. Experimental evaluation setup for OOD detection.

5.1. Empirical Results

ImageNet-1k benchmark: The ImageNet-1k benchmark is crucial for OOD evaluation, as large-scale datasets offer a comprehensive representation of real-world scenarios. Consequently, post-hoc methods are particularly valuable when training data is inaccessible and retraining is computationally prohibitive. We compare our proposed method, AdaSCALE, with recent state-of-the-art approaches across eight architectures on the ImageNet-1k benchmark, as presented in Table 1. AdaSCALE demonstrates consistently strong performance across all architectures compared to existing methods. Specifically, it surpasses the *best-generalizing* method, OptFS, by **14.94% / 8.96%** in the FPR@95/AUROC metric for near-OOD detection across all architectures. Additionally, it outperforms the *best-performing method*, SCALE (on ResNet-50), by **12.96% / 6.44%** in the same metric. A closer observation reveals that while OptFS excels in architectures such as EfficientNet, ViT-B-16, and Swin-B, scaling baselines perform comparably or even better in architectures like ResNet-50, ResNet-101, RegNet-Y-16, and DenseNet-201. In contrast, AdaSCALE-A achieves the best performance in near-OOD detection across all architectures, except for Swin-B, where BFAct performs optimally. Furthermore, the effectiveness of AdaSCALE extends beyond the near-OOD detection to far-OOD detection, demonstrating an average gain of **21.67%** in the FPR@95 metric compared to OptFS.

Full-Spectrum OOD Detection: Full-spectrum OOD (FS-OOD) detection extends conventional OOD detection by incorporating model’s ability to generalize on covariate-shifted ID inputs. We present FS-OOD detection results in Table 3. We can observe that this is a highly challenging task, as

Method	Near-OOD		Far-OOD	
	FPR@95 ↓	AUROC ↑	FPR@95 ↓	AUROC ↑
MSP	86.75	50.13	74.28	65.67
MLS	88.93	49.48	76.33	65.06
EBO	89.11	49.08	77.21	63.44
ReAct	87.22	51.38	67.23	69.53
ASH	87.01	52.02	72.36	65.70
SCALE	86.75	52.27	69.36	68.97
BFAc	87.12	51.14	66.13	69.69
LTS	86.46	53.29	66.76	71.63
OptFS	85.83	52.17	63.32	71.44
AdaSCALE-A	81.34	55.03	58.87	72.41
AdaSCALE-L	81.62	55.14	59.19	72.85

Table 3. Full-Spectrum OOD detection results on ImageNet-1k benchmark averaged over eight diverse architectures.

covariate-shifted ID datasets cause a significant performance drop for all methods compared to the conventional case. Despite this, AdaSCALE outperforms OptFS by **4.49** and **4.13** points on average in the FPR@95 metric for full-spectrum OOD detection across both near- and far-OOD datasets.

ISH training: Apart from enhancing the prior postprocessor ASH [7], SCALE [56] introduces a training regularization to emphasize samples with more distinct ID characteristics. We assess the performance of each method in ResNet-50 and ResNet-101 model following this regularization in Table 4. The results indicate that AdaSCALE maintains a substantial advantage, surpassing the second-best method, SCALE, by **12.56%/5.82%** and **20.46%/1.21%** in FPR@95 / AUROC for near- and far-OOD detection in ResNet-50, respectively. Moreover, AdaSCALE demonstrates superior performance beyond conventional OOD detection, with corresponding improvements of **4.10%/5.87%** and **9.70%/1.12%** in a full-spectrum setting. Furthermore, ISH regularization further amplifies the performance gap between AdaSCALE-A and OptFS, enhancing the near-OOD detection improvement from 12.96% / 6.44% to **15.18%/14.83%**. These findings also seem to generalize to the ResNet-101 network, as shown in Table 4.

CIFAR benchmark: CIFAR benchmarks are traditionally used to evaluate OOD detectors in smaller-scale settings. We compare AdaSCALE with recent state-of-the-art post-hoc baselines on CIFAR benchmarks using WRN-28-10 and DenseNet-101 networks, reporting the averaged performance over both architectures in Table 5. AdaSCALE outperforms all methods in average AUROC metric across CIFAR benchmarks in both near- and far-OOD detection. For far-OOD detection on CIFAR-10 benchmark, AdaSCALE-A achieves the best FPR@95 score of **33.11**, outperforming the MSP baseline by approximately 1.4 points. Similarly, AdaSCALE-A attains the best FPR@95 / AUROC of **43.07 / 90.31** in near-OOD detection, though MSP remains competitive. In near-OOD detection on CIFAR-100 benchmark,

Method	OOD Detection		FS-OOD Detection	
	Near-OOD	Far-OOD	Near-OOD	Far-OOD
ResNet-50				
MSP	74.07 / 62.16	51.13 / 84.64	87.52 / 40.36	74.41 / 61.52
MLS	74.38 / 66.43	41.57 / 88.90	88.89 / 39.49	71.53 / 61.69
EBO	74.68 / 66.46	41.85 / 88.83	89.05 / 39.18	71.77 / 61.11
ReAct	71.98 / 70.81	28.76 / 93.49	87.78 / 43.88	61.87 / 71.64
ASH	67.99 / 73.46	23.88 / 94.67	85.74 / 45.29	57.81 / 72.81
SCALE	65.68 / 76.41	20.77 / 95.62	84.31 / 48.40	54.48 / 74.79
BFAc	71.59 / 70.85	28.38 / 93.50	87.51 / 43.95	61.39 / 71.43
LTS	66.32 / 75.03	22.07 / 95.28	85.08 / 46.16	57.11 / 73.06
OptFS	67.71 / 73.03	24.65 / 94.18	85.38 / 45.91	57.09 / 72.95
AdaSCALE-A	57.43 / 80.86	16.52 / 96.46	80.85 / 51.24	51.57 / 75.63
AdaSCALE-L	56.83 / 80.81	17.62 / 96.22	80.97 / 50.59	53.43 / 74.62
ResNet-101				
MSP	71.39 / 68.31	51.00 / 84.81	85.70 / 45.72	73.69 / 62.79
MLS	72.32 / 71.94	41.04 / 88.99	87.39 / 44.88	69.94 / 63.23
EBO	72.78 / 71.92	41.45 / 88.87	87.64 / 44.66	70.23 / 62.65
ReAct	67.74 / 75.74	28.53 / 93.47	85.40 / 48.83	60.50 / 72.18
ASH	66.03 / 77.79	25.21 / 94.43	83.95 / 50.57	56.91 / 73.37
SCALE	64.30 / 78.98	23.09 / 94.95	83.14 / 51.05	55.88 / 73.27
BFAc	67.53 / 75.86	28.32 / 93.40	85.11 / 48.96	60.12 / 71.83
LTS	66.32 / 75.03	22.07 / 95.28	85.08 / 46.16	57.11 / 73.06
OptFS	67.71 / 73.03	24.65 / 94.18	85.38 / 45.91	57.09 / 72.95
AdaSCALE-A	54.66 / 83.52	16.81 / 96.32	78.52 / 55.19	49.92 / 76.20
AdaSCALE-L	53.91 / 83.49	17.55 / 96.15	78.63 / 54.60	51.47 / 75.47

Table 4. OOD detection results (FPR@95 ↓ / AUROC ↑) on ImageNet-1k benchmark with ISH [54] regularization.

AdaSCALE-A achieves the highest AUROC of **81.35**, while in far-OOD detection, AdaSCALE-L reaches the best performance with FPR@95 / AUROC of **52.49 / 82.21**. While activation-shaping methods (ReAct, ASH, SCALE, OptFS) perform remarkably well in comparison to logit-based methods in a large-scale setting (ImageNet-1k), they generally seem to underperform in small-scale settings (CIFAR). In contrast, AdaSCALE’s achieves consistently superior performance across all setups, demonstrating its robustness.

Accuracy: Like SCALE and LTS, AdaSCALE applies linear transformations to scale activations or logits, preserving accuracy, unlike post-hoc rectification methods [7, 47].

Method	CIFAR-10		CIFAR-100	
	Near-OOD	Far-OOD	Near-OOD	Far-OOD
MSP	43.18 / 89.07	34.49 / 90.88	55.64 / 80.23	61.73 / 76.82
MLS	51.54 / 89.33	39.62 / 91.68	57.24 / 81.25	60.19 / 78.92
EBO	51.54 / 89.37	39.58 / 91.75	57.45 / 81.10	60.12 / 78.96
ReAct	49.71 / 88.59	37.32 / 92.00	63.20 / 79.58	54.78 / 80.46
ASH	78.11 / 77.97	63.12 / 83.35	80.97 / 70.09	69.38 / 79.06
SCALE	53.00 / 89.20	39.27 / 91.93	58.38 / 81.00	57.19 / 80.56
BFAc	54.90 / 88.56	43.05 / 90.66	72.26 / 74.70	57.44 / 77.63
LTS	55.71 / 88.77	41.06 / 91.74	59.98 / 80.60	80.48 / 81.79
OptFS	64.82 / 85.72	47.67 / 89.99	76.80 / 73.02	60.23 / 77.76
AdaSCALE-A	43.07 / 90.31	33.11 / 92.66	57.33 / 81.35	54.53 / 81.14
AdaSCALE-L	44.71 / 90.14	33.43 / 92.69	58.70 / 81.07	52.49 / 82.21

Table 5. OOD detection results (FPR@95 ↓ / AUROC ↑) averaged over WRN-28-10 and DenseNet-101 networks on CIFAR benchmarks across 3 trials. (See Appendix D for complete results.)

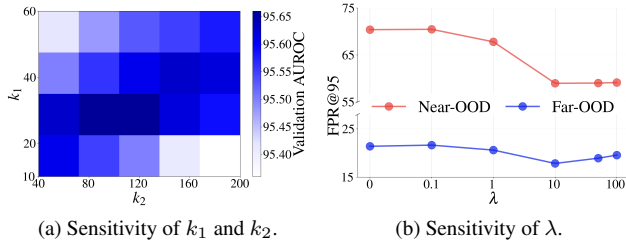


Figure 6. Sensitivity analysis with ResNet-50 (ImageNet-1k).

5.2. Ablation / hyperparameter studies

Sensitivity of k_1 , k_2 , and λ . As discussed in Sec. 4.1.2, ID and OOD distinctions are more pronounced in high activations but diminish as more activations are included. We analyze the impact of k_1 (used in activation shift) and k_2 (used in perturbed activation) using a heatmap of validation AUROC with ResNet-50 (Figure 6a). The darker region indicates higher AUROC, suggesting optimal values of $k_1 \approx 1\%$ (20) and $k_2 \approx 5\%$ (100) for ResNet-50 model. Furthermore, the heatmap suggests that k_1 is far more critical hyperparameter than k_2 . The hyperparameter λ controls the weighting of Q in computing Q' , the predetermined OOD likelihood. The sensitivity analysis is presented in Figure 6b which shows near-OOD and far-OOD detection using FPR@95. It suggests optimal FPR@95 is achieved at $\lambda \approx 10$.

Predetermined OOD likelihood Q' . Adaptive scaling depends on predetermined OOD likelihood to determine the extent of scaling. We study the effect of various predetermined OOD likelihood functions on OOD detection using ResNet-50 network (ImageNet-1k) in Table 6. It clearly shows Q component of Q' being most critical while $\sum_{k=1}^{k_2} \mathbf{a}_{\text{argsort}(\mathbf{a})_k}^\epsilon$ as correction term being a relatively superior choice.

Q'	OOD Detection	
	Near-OOD	Far-OOD
Q	59.43 / 78.14	19.70 / 95.73
$\sum_{k=1}^{k_2} \mathbf{a}_{\text{argsort}(\mathbf{a})_k}^\epsilon$	70.39 / 74.00	21.40 / 95.31
$\lambda \cdot Q + \sum_{k=1}^{k_2} \mathbf{a}_{\text{argsort}(\mathbf{a})_k}^\epsilon$	58.97 / 78.98	17.84 / 96.14
$\sum_{k=1}^{k_2} \max_k(\mathbf{a})$	65.11 / 76.23	19.76 / 95.67
$\lambda \cdot Q + \sum_{k=1}^{k_2} \max_k(\mathbf{a})$	58.91 / 78.74	18.02 / 96.08

Table 6. Ablation studies of Q' in FPR@95 \downarrow / AUROC \uparrow format.

Adaptive percentile. Unlike SCALE which uses constant percentile, AdaSCALE uses dynamic percentile lying in $[p_{\min}, p_{\max}]$ range adaptive to each sample. We show the effect of various percentile limit ranges in Figure 7 in the form of a heatmap on the AUROC validation metric on ImageNet-1k benchmark. The extent of darkness in the heatmap conveys a strong performance (corresponding to

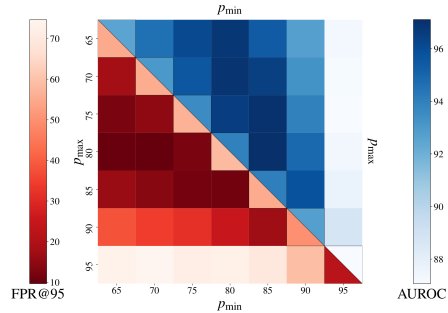


Figure 7. OOD detection performance (FPR@95 \downarrow / AUROC \uparrow) on ImageNet-1k with varying p_{\min} and p_{\max} . Diagonal entries ($p_{\min} = p_{\max}$) represent SCALE, while rest entries represent AdaSCALE.

highest AUROC / lowest FPR@95). The diagonal entries, representing the results of SCALE, are lighter in comparison to the rest of the cells, denoting the results of AdaSCALE. Hence, it can be observed that using adaptive percentile leads to better OOD detection in comparison to static percentile.

ID statistics. With the rise of large models, where training data is often undisclosed or inaccessible, relying on full training ID datasets for OOD detection has become increasingly impractical. While our approach leverages ID statistics for optimal performance, we rigorously assess its effectiveness with limited data. We conduct experiments on ImageNet-1k using n_{val} ID samples to compute ID statistics, where $n_{\text{val}} \in \{10, 100, 1000, 5000\}$. The results in Table 7 confirm that even with substantially restricted access to ID data, AdaSCALE-A achieves state-of-the-art performance.

n_{val}	OOD Detection		FS-OOD Detection	
	Near-OOD	Far-OOD	Near-OOD	Far-OOD
10	59.69 / 78.52	18.25 / 96.03	81.66 / 49.76	52.18 / 75.01
100	59.05 / 78.92	17.79 / 96.13	81.52 / 49.19	52.39 / 74.82
1000	58.99 / 78.95	17.86 / 96.13	81.55 / 49.48	52.24 / 74.94
5000	58.97 / 78.98	17.84 / 96.14	81.52 / 49.35	52.33 / 74.89

Table 7. Effectiveness of AdaSCALE-A with restricted access to ID data using ResNet-50 network in FPR@95 \downarrow / AUROC \uparrow format.

6. Conclusion

We propose **AdaSCALE**, a novel post-hoc OOD detection method that dynamically adjusts the scaling process based on a sample’s estimated OOD likelihood. Leveraging the observation that OOD samples exhibit larger activation shifts under minor perturbations, AdaSCALE assigns stronger scaling to likely ID samples and weaker scaling to likely OOD samples, enhancing ID-OOD separability. AdaSCALE achieves state-of-the-art performance as well as generalization across architectures requiring negligibly few ID samples, making it highly practical for real-world deployment.

References

- [1] Mouin Ben Ammar, Nacim Belkhir, Sebastian Popescu, Antoine Manzanera, and Gianni Franchi. NECO: NEural collapse based out-of-distribution detection. In *The Twelfth International Conference on Learning Representations (ICLR)*, 2024. 2
- [2] Eunsu Baek, Keondo Park, Jiyeon Kim, and Hyung-Sin Kim. Unexplored faces of robustness and out-of-distribution: Covariate shifts in environment and sensor domains. In *Proceedings of the IEEE/CVF Conference on Computer Vision and Pattern Recognition (CVPR)*, pages 22294–22303, 2024. 1
- [3] Yichen Bai, Zongbo Han, Bing Cao, Xiaoheng Jiang, Qinghua Hu, and Changqing Zhang. Id-like prompt learning for few-shot out-of-distribution detection. In *Proceedings of the IEEE/CVF Conference on Computer Vision and Pattern Recognition (CVPR)*, pages 17480–17489, 2024. 3
- [4] Sima Behpour, Thang Doan, Xin Li, Wenbin He, Liang Gou, and Liu Ren. Gradorth: A simple yet efficient out-of-distribution detection with orthogonal projection of gradients. In *Thirty-seventh Conference on Neural Information Processing Systems (NeurIPS)*, 2023. 2
- [5] Jingtang Chen, Junjie Li, Xiaoyang Qu, Jianzong Wang, Jiguang Wan, and Jing Xiao. GAIA: Delving into gradient-based attribution abnormality for out-of-distribution detection. In *Thirty-seventh Conference on Neural Information Processing Systems (NeurIPS)*, 2023. 2
- [6] Terrance DeVries and Graham W Taylor. Learning confidence for out-of-distribution detection in neural networks. *arXiv preprint arXiv:1802.04865*, 2018. 3
- [7] Andrija Djuricic, Nebojsa Bozanic, Arjun Ashok, and Rosanne Liu. Extremely simple activation shaping for out-of-distribution detection. In *The Eleventh International Conference on Learning Representations (ICLR)*, 2023. 1, 2, 5, 6, 7
- [8] Andrija Djuricic, Rosanne Liu, and Mladen Nikolic. Logit scaling for out-of-distribution detection. *arXiv preprint arXiv:2409.01175*, 2024. 1, 2, 3, 5, 6
- [9] Xuefeng Du, Zhaoning Wang, Mu Cai, and Yixuan Li. Vos: Learning what you don't know by virtual outlier synthesis. In *Proceedings of the International Conference on Learning Representations (ICLR)*, 2022. 3
- [10] Xuefeng Du, Yiyu Sun, Jerry Zhu, and Yixuan Li. Dream the impossible: Outlier imagination with diffusion models. *Advances in Neural Information Processing Systems (NeurIPS)*, 36:60878–60901, 2023. 3
- [11] Xuefeng Du, Zhen Fang, Ilias Diakonikolas, and Yixuan Li. How does unlabeled data provably help out-of-distribution detection? In *The Twelfth International Conference on Learning Representations (ICLR)*, 2024. 3
- [12] Heng Gao, Zhuolin He, Shoumeng Qiu, and Jian Pu. Oal: Enhancing ood detection using latent diffusion, 2024. 3
- [13] Ruiyuan Gao, Chenchen Zhao, Lanqing Hong, and Qiang Xu. Diffguard: Semantic mismatch-guided out-of-distribution detection using pre-trained diffusion models. In *Proceedings of the IEEE/CVF International Conference on Computer Vision (ICCV)*, pages 1579–1589, 2023. 3
- [14] Maximilian Granz, Manuel Heurich, and Tim Landgraf. Weiper: OOD detection using weight perturbations of class projections. In *The Thirty-eighth Annual Conference on Neural Information Processing Systems (NeurIPS)*, 2024. 2
- [15] Rundong He, Yue Yuan, Zhongyi Han, Fan Wang, Wan Su, Yilong Yin, Tongliang Liu, and Yongshun Gong. Exploring channel-aware typical features for out-of-distribution detection. In *Proceedings of the AAAI conference on artificial intelligence (AAAI)*, pages 12402–12410, 2024. 2
- [16] Dan Hendrycks and Kevin Gimpel. A baseline for detecting misclassified and out-of-distribution examples in neural networks. In *International Conference on Learning Representations (ICLR)*, 2017. 1, 2, 6
- [17] Dan Hendrycks, Mantas Mazeika, and Thomas Dietterich. Deep anomaly detection with outlier exposure. In *International Conference on Learning Representations (ICLR)*, 2019. 3
- [18] Dan Hendrycks, Mantas Mazeika, Saurav Kadavath, and Dawn Song. Using self-supervised learning can improve model robustness and uncertainty. In *Proceedings of the 33rd Conference on Neural Information Processing Systems (NeurIPS)*, 2019. 3
- [19] Dan Hendrycks*, Norman Mu*, Ekin Dogus Cubuk, Barret Zoph, Justin Gilmer, and Balaji Lakshminarayanan. Augmix: A simple method to improve robustness and uncertainty under data shift. In *International Conference on Learning Representations (ICLR)*, 2020. 3
- [20] Dan Hendrycks, Steven Basart, Mantas Mazeika, Mohamadreza Mostajabi, Jacob Steinhardt, and Dawn Song. Scaling out-of-distribution detection for real-world settings. In *International Conference on Machine Learning (ICML)*, 2022. 1, 2, 6
- [21] Dan Hendrycks, Andy Zou, Mantas Mazeika, Leonard Tang, Bo Li, Dawn Song, and Jacob Steinhardt. Pixmix: Dreamlike pictures comprehensively improve safety measures. In *Proceedings of the IEEE/CVF Conference on Computer Vision and Pattern Recognition (CVPR)*, pages 16783–16792, 2022. 3
- [22] Yen-Chang Hsu, Yilin Shen, Hongxia Jin, and Zsolt Kira. Generalized odin: Detecting out-of-distribution image without learning from out-of-distribution data. In *Proceedings of the IEEE/CVF Conference on Computer Vision and Pattern Recognition (CVPR)*, 2020. 3
- [23] Rui Huang, Andrew Geng, and Yixuan Li. On the importance of gradients for detecting distributional shifts in the wild. *Advances in Neural Information Processing Systems (NeurIPS)*, 34, 2021. 2
- [24] Jang-Hyun Kim, Sangdoon Yun, and Hyun Oh Song. Neural relation graph: a unified framework for identifying label noise and outlier data. *Advances in Neural Information Processing Systems (NeurIPS)*, 36, 2024. 1
- [25] Haojia Kong and Haoan Li. Bfact: Out-of-distribution detection with butterworth filter rectified activations. In *International Conference on Cognitive Systems and Signal Processing (ICCSIP)*, pages 115–129. Springer, 2022. 1, 2, 6
- [26] Gerhard Krumpl, Henning Avenhaus, Horst Possegger, and Horst Bischof. Ats: Adaptive temperature scaling for enhancing out-of-distribution detection methods. In *Proceedings of*

- the *IEEE/CVF Winter Conference on Applications of Computer Vision (WACV)*, pages 3864–3873, 2024. 1, 3
- [27] Kimin Lee, Kibok Lee, Honglak Lee, and Jinwoo Shin. A simple unified framework for detecting out-of-distribution samples and adversarial attacks. In *Advances in Neural Information Processing Systems (NeurIPS)*, 2018. 1, 2
- [28] Hengzhuang Li and Teng Zhang. Outlier synthesis via hamiltonian monte carlo for out-of-distribution detection. In *The Thirteenth International Conference on Learning Representations (ICLR)*, 2025. 3
- [29] Tianqi Li, Guansong Pang, Xiao Bai, Wenjun Miao, and Jin Zheng. Learning transferable negative prompts for out-of-distribution detection. In *Proceedings of the IEEE/CVF Conference on Computer Vision and Pattern Recognition (CVPR)*, pages 17584–17594, 2024. 3
- [30] Shiyu Liang, Yixuan Li, and Rayadurgam Srikant. Enhancing the reliability of out-of-distribution image detection in neural networks. In *International Conference on Learning Representations (ICLR)*, 2018. 1, 2, 6
- [31] Litian Liu and Yao Qin. Detecting out-of-distribution through the lens of neural collapse. *arXiv preprint arXiv:2311.01479*, 2023. 2
- [32] Litian Liu and Yao Qin. Fast decision boundary based out-of-distribution detector. In *International Conference on Machine Learning (ICML)*, 2024. 2
- [33] Weitang Liu, Xiaoyun Wang, John D. Owens, and Yixuan Li. Energy-based out-of-distribution detection. In *Proceedings of the 34th Conference on Neural Information Processing Systems (NeurIPS)*, 2020. 1, 2, 6
- [34] Xixi Liu, Yaroslava Lochman, and Christopher Zach. Gen: Pushing the limits of softmax-based out-of-distribution detection. In *Proceedings of the IEEE/CVF Conference on Computer Vision and Pattern Recognition*, 2023. 2
- [35] Haodong Lu, Dong Gong, Shuo Wang, Jason Xue, Lina Yao, and Kristen Moore. Learning with mixture of prototypes for out-of-distribution detection. In *The Twelfth International Conference on Learning Representations (ICLR)*, 2024. 3
- [36] Yifei Ming, Yiyu Sun, Ousmane Dia, and Yixuan Li. How to exploit hyperspherical embeddings for out-of-distribution detection? In *The Eleventh International Conference on Learning Representations (ICLR)*, 2023. 3
- [37] Jun Nie, Yadan Luo, Shanshan Ye, Yonggang Zhang, Xinmei Tian, and Zhen Fang. Out-of-distribution detection with virtual outlier smoothing. *International Journal of Computer Vision (IJCV)*, 2024. 3
- [38] Bartłomiej Olber, Krystian Radlak, Adam Popowicz, Michał Szczepankiewicz, and Krystian Chachula. Detection of out-of-distribution samples using binary neuron activation patterns. In *Proceedings of the IEEE/CVF Conference on Computer Vision and Pattern Recognition (CVPR)*, 2023. 2
- [39] Jaewoo Park, Yoon Gyo Jung, and Andrew Beng Jin Teoh. Nearest neighbor guidance for out-of-distribution detection. In *Proceedings of the IEEE/CVF International Conference on Computer Vision*, 2023. 2
- [40] Magesh Rajasekaran, Md Saiful Islam Sajol, Frej Berglind, Supratik Mukhopadhyay, and Kamalika Das. Combood: A semiparametric approach for detecting out-of-distribution data for image classification. In *Proceedings of the 2024 SIAM International Conference on Data Mining (SDM)*, pages 643–651. SIAM, 2024. 1, 2
- [41] Sudarshan Regmi. Going beyond conventional ood detection, 2024. 3
- [42] Sudarshan Regmi, Bibek Panthi, Sakar Dotel, Prashanna K Gyawali, Danail Stoyanov, and Binod Bhattacharai. T2fnorm: Train-time feature normalization for ood detection in image classification. In *Proceedings of the IEEE/CVF Conference on Computer Vision and Pattern Recognition (CVPR) Workshops*, 2024. 3
- [43] Sudarshan Regmi, Bibek Panthi, Yifei Ming, Prashanna K Gyawali, Danail Stoyanov, and Binod Bhattacharai. Reweightood: Loss reweighting for distance-based ood detection. In *Proceedings of the IEEE/CVF Conference on Computer Vision and Pattern Recognition (CVPR) Workshops*, 2024. 3
- [44] Jie Ren, Stanislav Fort, Jeremiah Liu, Abhijit Guha Roy, Shreyas Padhy, and Balaji Lakshminarayanan. A simple fix to mahalanobis distance for improving near-ood detection. *arXiv preprint arXiv:2106.09022*, 2021. 1, 2
- [45] Sina Sharifi, Taha Entesari, Bardia Safaei, Vishal M. Patel, and Mahyar Fazlyab. Gradient-regularized out-of-distribution detection. In *European Conference on Computer Vision (ECCV)*, pages 691–708, Cham, 2025. Springer. 2
- [46] Yiyu Sun and Yixuan Li. Dice: Leveraging sparsification for out-of-distribution detection. In *European Conference on Computer Vision (ECCV)*, pages 691–708. Springer, 2022. 1, 2
- [47] Yiyu Sun, Chuan Guo, and Yixuan Li. React: Out-of-distribution detection with rectified activations. *Advances in Neural Information Processing Systems (NeurIPS)*, 34, 2021. 1, 2, 3, 6, 7
- [48] Yiyu Sun, Yifei Ming, Xiaojin Zhu, and Yixuan Li. Out-of-distribution detection with deep nearest neighbors. *Proceedings of the 39th International Conference on Machine Learning (ICML)*, 2022. 1, 2
- [49] Leitian Tao, Xuefeng Du, Jerry Zhu, and Yixuan Li. Non-parametric outlier synthesis. In *The Eleventh International Conference on Learning Representations (ICLR)*, 2023. 3
- [50] Haoqi Wang, Zhizhong Li, Litong Feng, and Wayne Zhang. Vim: Out-of-distribution with virtual-logit matching. In *Proceedings of the IEEE/CVF Conference on Computer Vision and Pattern Recognition (CVPR)*, 2022. 1, 2
- [51] Hualiang Wang, Yi Li, Huifeng Yao, and Xiaomeng Li. Clipn for zero-shot ood detection: Teaching clip to say no. In *Proceedings of the IEEE/CVF International Conference on Computer Vision (ICCV)*, pages 1802–1812, 2023. 3
- [52] Hongxin Wei, Renchunzi Xie, Hao Cheng, Lei Feng, Bo An, and Yixuan Li. Mitigating neural network overconfidence with logit normalization. In *International Conference on Machine Learning (ICML)*. PMLR, 2022. 3
- [53] Haipeng Xiong, Kai Xu, and Angela Yao. Fixing data augmentations for out-of-distribution detection, 2024. 3
- [54] Kai Xu, Rongyu Chen, Gianni Franchi, and Angela Yao. Scaling for training time and post-hoc out-of-distribution detection enhancement. In *The Twelfth International Conference on Learning Representations (ICLR)*, 2024. 1, 2, 5, 6, 7

- [55] Mingyu Xu, Zheng Lian, Bin Liu, and Jianhua Tao. Vra: Variational rectified activation for out-of-distribution detection. *Advances in Neural Information Processing Systems (NeurIPS)*, 2023. 1, 2
- [56] Pingmei Xu, Krista A Ehinger, Yinda Zhang, Adam Finkelstein, Sanjeev R Kulkarni, and Jianxiong Xiao. Turkergaze: Crowdsourcing saliency with webcam based eye tracking. *arXiv preprint arXiv:1504.06755*, 2015. 7
- [57] Jingkang Yang, Pengyun Wang, Dejian Zou, Zitang Zhou, Kunyuan Ding, WenXuan Peng, Haoqi Wang, Guangyao Chen, Bo Li, Yiyu Sun, Xuefeng Du, Kaiyang Zhou, Wayne Zhang, Dan Hendrycks, Yixuan Li, and Ziwei Liu. OpenOOD: Benchmarking generalized out-of-distribution detection. In *Advances in Neural Information Processing Systems (NeurIPS), Datasets and Benchmarks Track*, 2022. 3, 6
- [58] Jingkang Yang, Kaiyang Zhou, and Ziwei Liu. Full-spectrum out-of-distribution detection. *International Journal of Computer Vision (IJCV)*, 2023. 1, 2
- [59] Jinsong Zhang, Qiang Fu, Xu Chen, Lun Du, Zelin Li, Gang Wang, xiaoguang Liu, Shi Han, and Dongmei Zhang. Out-of-distribution detection based on in-distribution data patterns memorization with modern hopfield energy. In *The Eleventh International Conference on Learning Representations (ICLR)*, 2023. 2
- [60] Jingyang Zhang, Nathan Inkawhich, Randolph Linderman, Yiran Chen, and Hai Li. Mixture outlier exposure: Towards out-of-distribution detection in fine-grained environments. In *Proceedings of the IEEE/CVF Winter Conference on Applications of Computer Vision (WACV)*, 2023. 3
- [61] Jingyang Zhang, Jingkang Yang, Pengyun Wang, Haoqi Wang, Yueqian Lin, Haoran Zhang, Yiyu Sun, Xuefeng Du, Kaiyang Zhou, Wayne Zhang, et al. Openood v1. 5: Enhanced benchmark for out-of-distribution detection. *arXiv preprint arXiv:2306.09301*, 2023. 6, 3
- [62] Yonggang Zhang, Jie Lu, Bo Peng, Zhen Fang, and Yiu ming Cheung. Learning to shape in-distribution feature space for out-of-distribution detection. In *The Thirty-eighth Annual Conference on Neural Information Processing Systems (NeurIPS)*, 2024. 3
- [63] Yabin Zhang, Wenjie Zhu, Chenhang He, and Lei Zhang. Lapt: Label-driven automated prompt tuning for ood detection with vision-language models. In *European Conference on Computer Vision (ECCV)*, pages 271–288, Cham, 2025. Springer. 3
- [64] Qinyu Zhao, Ming Xu, Kartik Gupta, Akshay Asthana, Liang Zheng, and Stephen Gould. Towards optimal feature-shaping methods for out-of-distribution detection. In *The Twelfth International Conference on Learning Representations (ICLR)*, 2024. 1, 2, 3, 6
- [65] Jianing Zhu, Yu Geng, Jiangchao Yao, Tongliang Liu, Gang Niu, Masashi Sugiyama, and Bo Han. Diversified outlier exposure for out-of-distribution detection via informative extrapolation. In *Advances in Neural Information Processing Systems (NeurIPS)*, pages 22702–22734, 2023. 3
- [66] Yao Zhu, YueFeng Chen, Chuanlong Xie, Xiaodan Li, Rong Zhang, Hui Xue, Xiang Tian, Yaowu Chen, et al. Boosting out-of-distribution detection with typical features. *Advances in Neural Information Processing Systems (NeurIPS)*, 35: 20758–20769, 2022. 2
- [67] Zhipeng Zou, Sheng Wan, Guangyu Li, Bo Han, Tongliang Liu, Lin Zhao, and Chen Gong. Provable discriminative hyperspherical embedding for out-of-distribution detection. In *The AAAI Conference on Artificial Intelligence (AAAI)*, 2025. 3

AdaSCALE: Adaptive Scaling for OOD Detection

Supplementary Material

A. Notations

Table 8 lists all the notations used in this paper.

Notation	Meaning
\mathcal{X}	Input space.
\mathcal{Y}	Label space.
C	Number of classes.
C_{in}	Number of input channels.
h	Classifier.
$\mathcal{P}_{\text{ID}}(x, y)$	Underlying joint distribution of ID data.
$\mathcal{P}_{\text{OOD}}(x)$	Distribution of OOD data.
\mathcal{D}_{ID}	ID training dataset.
N	Number of training samples.
f_{θ}	Feature extractor, parameterized by θ .
\mathcal{A}	Activation space.
$g_{\mathcal{W}}$	Classifier (mapping activations to logits), parameterized by \mathcal{W} .
\mathcal{Z}	Logit space.
\mathbf{a}	Activation vector (output of $f_{\theta}(x)$).
a_j	The j -th element of the activation vector \mathbf{a} .
\mathbf{z}	Logit vector (output of $g_{\mathcal{W}}(\mathbf{a})$).
\mathcal{L}	Loss function (e.g., cross-entropy).
$S(x)$	OOD scoring function.
τ	Threshold for classifying an input as ID or OOD.
x	Input image.
$x[c, h, w]$	Channel value of input image x at position (c, h, w) .
H	Height of the input image.
W	Width of the input image.
$AT(x, c, h, w)$	Attribution function, assigning a score to each channel value of input x .
o	Percent of channel values to perturb.
R	Set of channel value indices with lowest absolute attribution scores.
y_{pred}	Predicted class index.
ε	Perturbation magnitude.
x^{ε}	Perturbed input image.
\mathbf{a}^{ε}	Activation vector of the perturbed input x^{ε} .
$\mathbf{a}^{\text{shift}}$	Activation shift vector (absolute element-wise difference between \mathbf{a} and \mathbf{a}^{ε}).
k_1, k_2	Number of highest-magnitude activations considered for Q and C_o , respectively.
$\text{argsort}(\mathbf{v})$	Same as $\text{argsort}(\mathbf{v}, \text{desc} = \text{True})$.
$\max_k(\mathbf{v})$	Returns the indices that would sort the vector \mathbf{v} in descending order.
$\mathbf{i}_1, \mathbf{i}_2$	Returns the k^{th} maximum element of vector \mathbf{v} .
Q	Index sets: $\mathbf{i}_1 = \text{argsort}(\mathbf{a}, \text{desc} = \text{True})[:k_1]$, $\mathbf{i}_2 = \text{argsort}(\mathbf{a}, \text{desc} = \text{True})[:k_2]$
C_o	Sum of activation shifts for the top- k_1 activations.
λ	Correction term: sum of top- k_2 perturbed activations.
Q'	Weighting factor for Q in the Q' calculation.
n_{val}	Estimated OOD likelihood.
\bar{Q}_s	Number of ID validation samples.
$F_{Q'}(Q')$	Set of Q' values on the ID validation samples.
$p_{\text{min}}, p_{\text{max}}$	Empirical cumulative distribution function (eCDF) of Q' values.
p_r	Minimum and maximum percentile thresholds.
p	Raw ID likelihood from eCDF
$P_p(\mathbf{a})$	Adjusted percentile threshold
r	The p -th percentile value of all elements in \mathbf{a}
$\mathbf{a}^{\text{scaled}}$	Scaled activation vector (AdaSCALE-A).
$\mathbf{z}^{\text{scaled}}$	Scaled logit vector (AdaSCALE-L).
$\text{ReLU}(a_j)$	Rectified Linear Unit activation function: $\text{ReLU}(a_j) = \max(0, a_j)$.

Table 8. Table of Notations

B. Additional studies

Image Perturbation. A sufficiently small perturbation, as discussed in Sec. 4.3, is used to make distinctive observations in ID vs OOD. We now systematically investigate the impact of the extent and nature of perturbation on pre-determining OOD likelihood which is in-turn responsible for OOD detection. We present the results in Table 9. It is clearly evident that perturbing regions with trivial intensity value leads to better OOD detection. We can infer that with such perturbation, Q' acts as a more reliable proxy for OOD likelihood. Another key takeaway is that randomly perturbing small regions can also lead to strong performance. This finding highlights a more efficient approach to OOD detection, relying solely on minor random perturbations rather than requiring a predetermination of trivial pixels. Furthermore, the sensitivity study of ε presented at Table 10 suggests the optimal value of ε to be around 0.5.

Region type	o%	OOD Detection		FS-OOD Detection	
		Near-OOD	Far-OOD	Near-OOD	Far-OOD
Random	1%	61.73 / 78.15	19.44 / 95.74	83.19 / 48.59	53.45 / 74.10
	5%	59.97 / 78.67	18.14 / 96.06	81.92 / 49.19	52.35 / 74.84
	10%	60.27 / 78.02	18.45 / 96.00	82.07 / 48.62	52.84 / 74.70
	50%	62.81 / 76.27	19.95 / 95.70	83.40 / 46.55	54.94 / 73.42
Trivial	1%	61.77 / 78.29	19.28 / 95.77	82.92 / 48.86	53.34 / 74.24
	5%	58.97 / 78.98	17.84 / 96.14	81.52 / 49.35	52.33 / 74.89
	10%	60.24 / 78.17	17.94 / 96.08	82.19 / 48.59	52.59 / 74.77
	50%	66.43 / 74.10	21.58 / 95.29	85.26 / 44.86	56.56 / 72.82
Significant	1%	69.43 / 75.13	22.62 / 95.17	85.59 / 48.32	53.76 / 75.23
	5%	67.31 / 75.78	21.24 / 95.44	85.07 / 48.40	53.26 / 75.63
	10%	65.65 / 76.20	20.39 / 95.62	84.36 / 48.33	53.17 / 75.55
	50%	64.54 / 75.39	20.48 / 95.61	83.78 / 47.07	54.11 / 74.54
All	100%	67.37 / 73.08	22.93 / 95.01	85.66 / 44.00	57.80 / 72.19

Table 9. Image perturbation study with ResNet-50 model in (FPR@95 ↓ / AUROC ↑) format on ImageNet-1k benchmark.

ε	Near-OOD		Far-OOD	
	FPR@95 ↓	AUROC ↑	FPR@95 ↓	AUROC ↑
0.1	63.76	77.50	19.26	95.85
0.5	58.97	78.98	17.84	96.14
1.0	61.60	76.96	19.31	95.84

Table 10. Sensitivity study of ε in conventional OOD detection with ResNet-50 model on ImageNet-1k benchmark.

Latency. AdaSCALE incurs extra computational overhead in comparison to its preceding works [7, 8, 54]. It uses an extra forward pass to obtain perturbed activation \mathbf{a}^ε . On top of that, top-k operations (time complexity: $\mathcal{O}(D \log D)$, where D is dimension of activation space) on Q and C_o are employed for pre-determining OOD likelihood. Furthermore, comparing variable percentile to fixed percentile for scaling in Table 11 across 10000 trials, we observe variable percentile inducing relatively higher latency. The latency ratio decreases as activation space with a higher dimension is considered. All experiments are performed using NVIDIA RTX 4090 GPUs.

	$d = 128$	$d = 512$	$d = 1024$	$d = 2048$	$d = 3024$
Fixed percentile (SCALE)	33 μ s	40 μ s	45 μ s	48 μ s	54 μ s
Variable percentile (AdaSCALE)	152 μ s	149 μ s	155 μ s	152 μ s	164 μ s
Latency ratio (AdaSCALE / SCALE)	4.66	3.76	3.42	3.14	3.02

Table 11. Latency with fixed vs. variable percentile for scaling.

C. Hyperparameters

All hyperparameters are determined with respect to the AUROC metric using automatic parameter search of OpenOOD [57, 61]. Although AdaSCALE may appear to require numerous hyperparameters, our findings indicate that setting $(\lambda, k_1, k_2, o, \epsilon)$ to $(10, 1\%, 5\%, 5\%, 0.5)$ consistently yields near-optimal performance across all setups. Consequently, it can be inferred that only the hyperparameters p_{\min} and p_{\max} need to be appropriately tuned for any new architecture for near-optimal performance.

Dataset	Network	Hyperparameters						
		p_{\min}	p_{\max}	λ	k_1	k_2	o	ϵ
CIFAR-10	WideResNet-28-10	60	95	10	1%	80%	5%	0.5
	DenseNet-101	65	90	10	1%	10%	5%	0.5
CIFAR-100	WideResNet-28-10	60	85	10	1%	80%	5%	0.5
	DenseNet-101	70	80	10	1%	100%	5%	0.5
ImageNet-1k	ResNet-50	80	85	10	1%	5%	5%	0.5
	ResNet-101	80	85	10	1%	5%	5%	0.5
	RegNet-Y-16	60	90	10	1%	50%	5%	0.5
	ResNeXt-50	80	85	10	1%	5%	5%	0.5
	DenseNet-201	90	95	10	1%	10%	5%	0.5
	EfficientNetV2-L	60	99	10	1%	20%	5%	0.5
	Vit-B-16	60	85	10	1%	100%	5%	0.5
	Swin-B	90	99	10	1%	5%	5%	0.5

Table 12. Hyperparameters used for each dataset and network for AdaSCALE-A.

Dataset	Network	Hyperparameters						
		p_{\min}	p_{\max}	λ	k_1	k_2	o	ϵ
CIFAR-10	WideResNet-28-10	60	85	10	1%	80%	5%	0.5
	DenseNet-101	70	85	10	1%	10%	5%	0.5
CIFAR-100	WideResNet-28-10	60	80	10	1%	80%	5%	0.5
	DenseNet-101	65	75	10	1%	50%	5%	0.5
ImageNet-1k	ResNet-50	80	85	10	1%	5%	5%	0.5
	ResNet-101	70	80	10	1%	5%	5%	0.5
	RegNet-Y-16	60	85	10	1%	5%	5%	0.5
	ResNeXt-50	70	80	10	1%	5%	5%	0.5
	DenseNet-201	90	95	10	1%	10%	5%	0.5
	EfficientNetV2-L	60	99	10	1%	5%	5%	0.5
	Vit-B-16	75	85	10	1%	100%	5%	0.5
	Swin-B	90	99	10	1%	100%	5%	0.5

Table 13. Hyperparameters used for each dataset and network for AdaSCALE-L.

D. CIFAR-results

D.1. WRN-28-10

<i>CIFAR-10 benchmark</i>					
Method	MNIST	SVHN	Textures	Places365	Average
MSP	17.02 / 94.61	21.71 / 92.96	60.50 / 88.06	42.27 / 90.04	35.38 / 91.42
MLS	<u>13.01 / 96.76</u>	30.35 / 93.06	76.12 / 86.65	52.56 / 90.46	43.01 / 91.73
EBO	12.93 / 96.93	30.35 / 93.12	76.15 / 86.68	52.57 / 90.56	43.00 / 91.82
ReAct	15.50 / 96.30	34.01 / 92.47	<u>57.76 / 88.77</u>	57.33 / 89.66	41.15 / 91.80
ASH	50.11 / 88.80	89.90 / 74.76	95.07 / 72.91	92.22 / 70.06	81.82 / 76.63
SCALE	13.24 / 96.70	32.21 / 92.88	75.76 / 86.77	55.81 / 90.09	44.26 / 91.61
BFAct	25.79 / 94.64	43.08 / 91.10	57.16 / 88.80	61.00 / 88.32	46.75 / 90.71
LTS	14.04 / 96.60	39.85 / 92.21	76.85 / 86.43	63.13 / 89.19	48.47 / 91.11
OptFS	25.68 / 94.83	51.58 / 89.86	62.14 / 88.07	80.19 / 84.05	54.90 / 89.20
AdaSCALE-A	14.93 / 96.02	17.84 / 95.14	64.96 / 88.31	34.57 / 92.31	33.08 / 92.95
AdaSCALE-L	15.58 / 95.98	<u>18.41 / 95.10</u>	62.87 / 88.67	<u>37.59 / 91.97</u>	<u>33.61 / 92.93</u>

<i>CIFAR-100 benchmark</i>					
	MNIST	SVHN	Textures	Places365	Average
MSP	49.79 / 78.72	56.76 / 80.70	64.49 / 76.86	<u>56.66 / 79.96</u>	56.92 / 79.06
MLS	46.57 / 81.43	53.08 / 83.37	64.59 / 77.65	59.70 / 79.82	55.99 / 80.57
EBO	46.41 / 81.99	52.92 / 83.77	64.58 / 77.61	59.76 / 79.60	55.92 / 80.74
ReAct	49.92 / 81.07	40.66 / 86.49	52.42 / 80.81	60.35 / 79.72	50.84 / 82.03
ASH	44.06 / <u>85.55</u>	41.48 / 87.50	61.78 / 81.65	80.45 / 71.83	56.94 / 81.63
SCALE	<u>40.65 / 84.68</u>	48.56 / 85.56	58.45 / 80.81	60.51 / 79.90	52.04 / 82.74
BFAct	61.59 / 77.47	34.74 / 88.50	47.30 / 83.38	64.49 / 78.47	52.03 / 81.96
LTS	36.27 / 87.38	45.41 / 87.23	53.90 / 83.18	62.62 / 79.64	<u>49.55 / 84.36</u>
OptFS	57.61 / 79.47	37.04 / 86.43	53.02 / 80.43	70.44 / 76.77	54.53 / 80.78
AdaSCALE-A	45.18 / 81.69	<u>36.79 / 89.20</u>	55.93 / 81.93	56.48 / 81.55	48.59 / 83.59
AdaSCALE-L	42.13 / 83.58	32.44 / 91.02	<u>50.87 / 84.14</u>	57.83 / <u>81.51</u>	45.82 / 85.06

Table 14. Far-OOD detection results (FPR@95↓ / AUROC↑) on CIFAR-10 and CIFAR-100 benchmarks using the WRN-28-10 network, averaged over 3 trials. The overall average performance is reported. The best results are **bold**, and the second-best results are underlined.

Method	<i>CIFAR-10 benchmark</i>		<i>CIFAR-100 benchmark</i>		Average
	CIFAR-100	TIN	CIFAR-10	TIN	
MSP	54.13 / 88.28	<u>42.94 / 89.93</u>	56.83 / 80.42	48.82 / 83.39	<u>50.68 / 85.51</u>
MLS	67.10 / 87.72	55.91 / 89.90	58.99 / 80.98	49.27 / 84.01	57.82 / 85.65
EBO	67.04 / 87.77	55.88 / 89.97	<u>58.97 / 80.93</u>	49.39 / 83.95	57.82 / 85.66
ReAct	65.96 / 87.76	51.44 / 90.33	69.17 / 79.10	51.56 / 83.77	59.53 / 85.24
ASH	91.33 / 70.72	90.77 / 73.28	85.25 / 69.96	78.31 / 74.55	86.42 / 72.13
SCALE	69.52 / 87.35	59.48 / 89.53	61.30 / 80.35	51.25 / 83.65	60.39 / 85.22
BFAct	66.31 / 86.94	57.12 / 89.69	78.90 / 74.98	59.04 / 82.25	65.34 / 83.47
LTS	74.28 / 86.38	66.01 / 88.56	64.17 / 79.57	54.24 / 83.09	64.68 / 84.40
OptFS	76.36 / 84.05	66.73 / 86.56	85.40 / 75.55	64.11 / 80.99	73.15 / 79.83
AdaSCALE-A	50.60 / 89.40	42.80 / 91.13	62.21 / 79.99	47.11 / 84.98	50.68 / 86.38
AdaSCALE-L	<u>53.98 / 89.01</u>	<u>45.95 / 90.77</u>	65.41 / 79.27	<u>48.74 / 84.75</u>	<u>53.52 / 85.95</u>

Table 15. Near-OOD detection results (FPR@95↓ / AUROC↑) on CIFAR-10 and CIFAR-100 benchmarks using the WRN-28-10 network, averaged over 3 trials. The overall average performance is reported. The best results are **bold**, and the second-best results are underlined.

D.2. DenseNet-101

<i>CIFAR-10 benchmark</i>					
Method	MNIST	SVHN	Textures	Places365	Average
MSP	17.91 / 94.22	32.04 / 90.38	46.80 / 87.53	37.59 / 89.24	33.59 / 90.34
MLS	10.02 / 97.58	31.25 / 92.59	64.43 / 85.58	39.19 / 90.74	36.22 / 91.62
EBO	9.74 / 97.76	31.23 / 92.69	64.46 / 85.48	39.17 / 90.81	36.15 / 91.68
ReAct	12.60 / 97.24	34.79 / 92.02	<u>50.41</u> / <u>88.21</u>	36.12 / 91.35	33.48 / 92.20
ASH	9.40 / 98.12	39.42 / 91.25	70.95 / 85.39	57.90 / 85.48	44.42 / 90.06
SCALE	9.04 / 97.88	26.99 / 93.54	61.52 / 86.77	39.57 / 90.76	34.28 / 92.24
BFAct	23.59 / 94.96	42.49 / 89.00	53.74 / 87.38	37.53 / 91.09	39.34 / 90.61
LTS	8.92 / <u>97.97</u>	27.16 / 93.59	59.07 / 87.09	39.47 / 90.81	33.65 / <u>92.37</u>
OptFS	9.74 / 97.88	41.20 / 90.71	51.35 / 88.48	59.47 / 86.03	40.44 / 90.77
AdaSCALE-A	12.42 / 96.85	25.04 / 94.05	58.28 / 87.35	<u>36.77</u> / <u>91.20</u>	33.13 / 92.36
AdaSCALE-L	10.92 / 97.44	<u>26.43</u> / <u>93.87</u>	58.59 / 87.19	37.03 / 91.25	<u>33.24</u> / 92.44
<i>CIFAR-100 benchmark</i>					
MSP	65.65 / 72.43	63.81 / 76.52	75.34 / 72.19	<u>61.36</u> / 77.16	66.54 / 74.57
MLS	58.69 / 78.55	57.12 / 79.43	79.05 / 72.68	62.72 / 78.38	64.39 / 77.26
EBO	58.58 / 78.98	56.76 / 79.19	79.09 / 72.44	62.86 / 78.08	64.32 / 77.17
ReAct	62.71 / 76.37	48.48 / 81.64	64.65 / <u>78.62</u>	59.00 / 78.89	<u>58.71</u> / 78.88
ASH	40.69 / 88.57	48.03 / 86.24	<u>65.24</u> / 83.29	73.29 / 71.88	56.81 / 82.49
SCALE	56.92 / 79.53	53.81 / 80.96	76.10 / 74.47	62.49 / 78.51	62.33 / 78.37
BFAct	73.83 / 67.19	60.01 / 75.85	69.29 / 76.41	68.15 / 73.73	67.82 / 73.29
LTS	<u>55.33</u> / <u>80.58</u>	51.33 / 82.04	73.06 / 75.89	62.58 / 78.36	60.58 / 79.22
OptFS	64.24 / 75.24	59.81 / 76.46	66.15 / 77.50	73.47 / 69.76	65.92 / 74.74
AdaSCALE-A	62.51 / 74.96	<u>46.29</u> / 84.31	71.40 / 76.59	61.70 / <u>78.86</u>	60.47 / 78.68
AdaSCALE-L	61.33 / 75.73	43.97 / <u>85.30</u>	69.31 / 77.71	61.97 / 78.69	59.15 / <u>79.36</u>

Table 16. Far-OOD detection results (FPR@95↓ / AUROC↑) on CIFAR-10 and CIFAR-100 benchmarks using the DenseNet-101 network, averaged over 3 trials. The overall average performance is reported. The best results are **bold**, and the second-best results are underlined.

Method	<i>CIFAR-10 benchmark</i>		<i>CIFAR-100 benchmark</i>		Average
	CIFAR-100	TIN	CIFAR-10	TIN	
MSP	40.13 / 88.45	35.50 / 89.61	59.94 / 77.53	56.96 / 79.57	48.13 / 83.79
MLS	45.14 / 88.85	38.01 / 90.85	<u>63.61</u> / 78.26	57.09 / 81.75	50.96 / 84.93
EBO	45.19 / 88.85	38.05 / 90.90	63.90 / 77.94	57.53 / 81.58	51.17 / 84.82
ReAct	44.34 / 89.19	37.10 / 91.08	70.77 / 75.06	61.30 / 80.40	53.38 / 83.93
ASH	67.78 / 82.68	62.54 / 85.18	81.65 / 65.84	78.66 / 70.01	72.66 / 75.93
SCALE	45.25 / 88.92	37.76 / 91.01	64.20 / <u>78.13</u>	56.96 / 81.88	51.04 / 84.99
BFAct	52.06 / 87.70	44.09 / 89.89	79.31 / 67.39	71.79 / 74.18	61.81 / 79.79
LTS	44.89 / 89.03	37.67 / 91.10	64.66 / 77.87	56.83 / 81.87	51.01 / 84.97
OptFS	60.63 / 85.29	55.55 / 86.96	82.97 / 64.99	74.73 / 70.55	68.47 / 76.95
AdaSCALE-A	43.29 / <u>89.37</u>	<u>35.57</u> / <u>91.32</u>	65.51 / 78.00	54.49 / <u>82.44</u>	<u>49.72</u> / 85.28
AdaSCALE-L	<u>43.19</u> / 89.40	35.70 / 91.37	66.09 / 77.79	<u>54.57</u> / 82.47	49.89 / <u>85.26</u>

Table 17. Near-OOD detection results (FPR@95↓ / AUROC↑) on CIFAR-10 and CIFAR-100 benchmarks using the DenseNet-101 network, averaged over 3 trials. The overall average performance is reported. The best results are **bold**, and the second-best results are underlined.

E. ImageNet-1k results

E.1. near-OOD detection

Method	SSB-Hard	NINCO	ImageNet-O	Average
MSP	74.49 / 72.09	56.88 / 79.95	91.32 / 28.60	74.23 / 60.21
MLS	76.20 / 72.51	59.44 / 80.41	88.97 / 40.73	74.87 / 64.55
EBO	76.54 / 72.08	60.58 / 79.70	88.84 / 41.78	75.32 / 64.52
REACT	77.55 / 73.03	55.82 / 81.73	84.45 / 51.67	72.61 / 68.81
ASH	73.66 / 72.89	53.05 / 83.45	81.70 / 57.67	69.47 / 71.33
SCALE	67.72 / 77.35	51.80 / 85.37	83.77 / 59.89	67.76 / 74.20
BFAct	77.20 / 73.15	55.27 / 81.88	84.57 / 51.62	72.35 / 68.88
LTS	68.46 / 77.10	51.24 / 85.33	84.33 / 57.69	68.01 / 73.37
OptFS	78.32 / 71.01	52.09 / 82.51	78.56 / 59.40	69.66 / 70.97
AdaSCALE-A	57.96 / 81.68	44.92 / 87.15	74.06 / 68.12	58.98 / 78.98
AdaSCALE-L	<u>58.68 / 81.42</u>	<u>45.01 / 87.11</u>	<u>75.83 / 67.33</u>	<u>59.84 / 78.62</u>

Table 18. Near-OOD detection results (FPR@95↓ / AUROC↑) on ImageNet-1k benchmark using ResNet-50 network. The best results are **bold**, and the second-best results are underlined.

Method	SSB-Hard	NINCO	ImageNet-O	Average
MSP	73.20 / 72.57	55.27 / 80.61	87.42 / 48.57	71.96 / 67.25
MLS	74.68 / 74.37	55.65 / 82.29	85.81 / 57.89	72.05 / 71.51
EBO	74.96 / 74.12	56.33 / 81.79	85.66 / 58.72	72.32 / 71.54
REACT	75.96 / 74.43	52.58 / 83.27	75.67 / 67.31	68.07 / 75.00
ASH	72.48 / 74.23	49.41 / 84.62	73.84 / 70.98	65.24 / 76.61
SCALE	68.47 / 77.10	49.03 / 86.20	74.09 / 72.50	63.87 / 78.60
BFAct	75.48 / 74.74	52.23 / 83.37	76.16 / 67.37	67.96 / 75.16
OptFS	76.55 / 72.29	50.89 / 83.35	68.94 / 71.85	65.46 / 75.83
AdaSCALE-A	61.00 / 80.29	46.70 / 86.99	<u>62.05 / 78.27</u>	<u>56.59 / 81.85</u>
AdaSCALE-L	<u>61.05 / 80.41</u>	<u>47.77 / 86.84</u>	60.40 / 78.35	56.41 / 81.86

Table 19. Near-OOD detection results (FPR@95↓ / AUROC↑) on ImageNet-1k benchmark using ResNet-101 network. The best results are **bold**, and the second-best results are underlined.

Method	SSB-Hard	NINCO	ImageNet-O	Average
MSP	65.35 / 78.28	48.48 / 86.85	72.82 / 77.09	62.22 / 80.74
MLS	62.48 / 84.83	42.76 / 91.56	83.60 / 77.58	62.94 / 84.66
EBO	<u>62.10</u> / <u>85.28</u>	<u>42.49</u> / <u>91.67</u>	83.82 / 77.33	62.80 / 84.76
REACT	73.02 / 73.17	59.81 / 80.91	79.37 / 72.02	70.73 / 75.37
ASH	80.58 / 67.70	77.23 / 71.42	89.71 / 64.30	82.51 / 67.81
SCALE	66.98 / 82.35	49.84 / 89.93	84.44 / 76.43	67.09 / 82.90
BFAct	79.40 / 64.39	73.98 / 70.35	82.76 / 63.54	78.72 / 66.09
LTS	69.52 / 79.78	55.38 / 87.71	84.55 / 74.78	69.82 / 80.75
OptFS	79.59 / 69.47	63.97 / 80.36	77.03 / 75.79	73.53 / 75.21
AdaSCALE-A	54.50 / 87.21	31.50 / 93.50	57.75 / 86.83	47.91 / 89.18
AdaSCALE-L	62.61 / 84.60	47.84 / 90.13	<u>57.94</u> / <u>86.61</u>	<u>56.13</u> / <u>87.11</u>

Table 20. Near-OOD detection results (FPR@95↓ / AUROC↑) on ImageNet-1k benchmark using RegNet-Y-16 network. The best results are **bold**, and the second-best results are underlined.

Method	SSB-Hard	NINCO	ImageNet-O	Average
MSP	73.04 / 73.28	57.90 / 80.86	88.81 / 49.43	73.25 / 67.86
MLS	74.68 / 75.06	60.79 / 81.91	86.87 / 57.87	74.11 / 71.61
EBO	74.90 / 74.89	60.96 / 81.44	86.76 / 58.49	74.21 / 71.61
REACT	75.54 / 74.51	57.29 / 82.50	80.03 / 65.37	70.95 / 74.13
ASH	70.72 / 76.64	58.40 / 83.49	83.84 / 65.63	70.99 / 75.25
SCALE	67.77 / 79.73	56.87 / 85.39	87.15 / 63.48	70.60 / 76.20
BFAct	75.36 / 74.65	57.65 / 82.46	79.86 / 65.30	70.96 / 74.14
LTS	68.26 / 79.36	56.35 / 85.39	86.22 / 63.85	70.28 / 76.20
OptFS	75.62 / 73.82	57.07 / 82.37	75.13 / 68.33	69.27 / 74.84
AdaSCALE-A	61.03 / 81.86	<u>50.80</u> / 86.54	80.57 / <u>71.48</u>	<u>64.13</u> / <u>79.96</u>
AdaSCALE-L	<u>61.57</u> / <u>81.11</u>	48.78 / <u>86.40</u>	<u>75.88</u> / 73.02	62.08 / 80.18

Table 21. Near-OOD detection results (FPR@95↓ / AUROC↑) on ImageNet-1k benchmark using ResNeXt-50 network. The best results are **bold**, and the second-best results are underlined.

Method	SSB-Hard	NINCO	ImageNet-O	Average
MSP	74.43 / 72.23	56.69 / 80.85	89.18 / 48.80	73.44 / 67.29
MLS	76.62 / 72.48	60.14 / 80.91	89.78 / 53.34	75.51 / 68.91
EBO	76.92 / 72.00	60.88 / 80.01	89.75 / 54.03	75.85 / 68.68
ReAct	78.62 / 70.93	57.51 / 81.19	73.78 / 68.83	69.97 / 73.65
ASH	78.80 / 68.71	63.84 / 79.45	80.07 / 68.19	74.24 / 72.12
SCALE	73.64 / 74.43	56.90 / 83.80	84.14 / 62.92	71.56 / 73.72
BFAct	81.57 / 67.52	65.10 / 77.38	66.93 / 72.93	71.20 / 72.61
LTS	73.46 / 74.36	57.54 / 83.79	82.87 / 65.52	71.29 / 74.56
OptFS	82.76 / 65.38	63.26 / 78.12	69.21 / 72.79	71.74 / 72.10
AdaSCALE-A	68.46 / 77.10	56.66 / 84.32	<u>58.72 / 77.55</u>	61.28 / 79.66
AdaSCALE-L	<u>68.97 / 76.85</u>	<u>57.96 / 83.92</u>	58.30 / 79.41	<u>61.75 / 80.06</u>

Table 22. Near-OOD detection results (FPR@95↓ / AUROC↑) on ImageNet-1k benchmark using DenseNet-201 network. The best results are **bold**, and the second-best results are underlined.

Method	SSB-Hard	NINCO	ImageNet-O	Average
MSP	81.28 / 75.03	57.97 / 86.70	78.26 / 80.53	72.51 / 80.76
MLS	84.74 / 73.50	72.88 / 84.83	86.71 / 79.32	81.44 / 79.22
EBO	85.27 / 71.58	75.81 / 82.07	87.49 / 77.81	82.86 / 77.15
ReAct	74.29 / 70.63	71.93 / 70.92	70.86 / 72.63	72.36 / 71.39
ASH	94.82 / 46.73	96.44 / 37.79	93.30 / 49.81	94.85 / 44.78
SCALE	90.16 / 57.07	89.93 / 59.69	89.03 / 63.60	89.70 / 60.12
BFAct	75.36 / 63.66	77.03 / 59.56	74.19 / 64.18	75.53 / 62.46
LTS	88.43 / 68.29	86.68 / 75.87	86.78 / 76.73	87.30 / 73.63
OptFS	74.68 / 73.83	70.24 / 76.18	71.94 / 75.86	72.29 / 75.29
AdaSCALE-A	<u>60.84 / 83.48</u>	47.45 / 89.47	<u>53.04 / 87.87</u>	53.78 / 86.94
AdaSCALE-L	53.56 / 85.00	<u>58.55 / 84.75</u>	<u>52.72 / 87.58</u>	<u>54.95 / 85.77</u>

Table 23. Near-OOD detection results (FPR@95↓ / AUROC↑) on ImageNet-1k benchmark using EfficientNetV2-L network. The best results are **bold**, and the second-best results are underlined.

Method	SSB-Hard	NINCO	ImageNet-O	Average
MSP	86.41 / 68.94	77.28 / 78.11	96.48 / 58.81	86.72 / 68.62
MLS	91.52 / 64.20	92.98 / 72.40	96.84 / 54.33	93.78 / 63.64
EBO	92.24 / 58.80	94.14 / 66.02	96.74 / 52.74	94.37 / 59.19
ReAct	90.46 / 63.10	78.50 / 75.43	90.94 / 66.53	86.63 / 68.35
ASH	93.50 / 53.90	95.37 / 52.51	94.47 / 53.19	94.45 / 53.20
SCALE	92.37 / 56.55	94.62 / 61.52	96.44 / 50.47	94.48 / 56.18
BFAct	89.81 / 64.16	71.37 / 78.06	85.09 / 69.75	82.09 / 70.66
LTS	91.42 / 64.35	82.63 / 75.48	92.42 / 62.46	88.83 / 67.43
OptFS	87.98 / 66.30	64.24 / <u>80.46</u>	77.43 / 71.43	76.55 / 72.73
AdaSCALE-A	85.89 / <u>66.57</u>	<u>61.92</u> / 80.47	67.81 / <u>72.37</u>	71.87 / <u>73.14</u>
AdaSCALE-L	<u>86.19</u> / 66.25	61.79 / 80.42	<u>67.99</u> / 73.01	<u>71.99</u> / 73.23

Table 24. Near-OOD detection results (FPR@95↓ / AUROC↑) on ImageNet-1k benchmark using ViT-B-16 network. The best results are **bold**, and the second-best results are underlined.

Method	SSB-Hard	NINCO	ImageNet-O	Average
MSP	86.47 / 71.30	77.95 / 78.50	96.90 / 59.65	87.11 / 69.82
MLS	94.05 / 65.04	93.38 / 71.75	96.97 / 57.26	94.80 / 64.68
EBO	94.66 / 58.96	94.59 / 64.02	96.75 / 56.40	95.34 / 59.79
ReAct	89.19 / 68.70	68.54 / 80.16	90.20 / 70.93	82.64 / 73.26
ASH	97.15 / 45.47	96.64 / 47.36	95.32 / 49.92	96.37 / 47.58
SCALE	90.84 / 56.53	87.86 / 62.49	87.16 / 65.38	88.62 / 61.47
BFAct	84.86 / 69.41	61.30 / 81.10	69.27 / 75.34	71.81 / 75.28
LTS	90.36 / 64.51	81.02 / 74.23	88.44 / 62.92	86.61 / 67.22
OptFS	88.68 / 68.43	66.36 / 80.27	75.38 / <u>73.49</u>	76.81 / 74.06
AdaSCALE-A	80.10 / 70.46	64.67 / <u>81.10</u>	75.46 / 71.87	73.41 / 74.48
AdaSCALE-L	<u>80.12</u> / <u>70.06</u>	63.68 / 81.35	<u>74.87</u> / 72.34	<u>72.89</u> / <u>74.58</u>

Table 25. Near-OOD detection results (FPR@95↓ / AUROC↑) on ImageNet-1k benchmark using Swin-B network. The best results are **bold**, and the second-best results are underlined.

E.2. far-OOD detection

Method	iNaturalist	Textures	OpenImage-O	Places	Average
MSP	43.34 / 88.41	60.87 / 82.43	50.13 / 84.86	58.26 / 80.55	53.15 / 84.06
MLS	30.61 / 91.17	46.17 / 88.39	37.88 / 89.17	55.62 / 84.05	42.57 / 88.19
EBO	31.30 / 90.63	45.77 / 88.70	38.09 / 89.06	55.73 / 83.97	42.72 / 88.09
ReAct	16.72 / 96.34	29.64 / 92.79	32.58 / 91.87	41.62 / 90.93	30.14 / 92.98
ASH	14.09 / 97.06	15.30 / 96.90	29.19 / 93.26	40.16 / 90.48	24.69 / 94.43
SCALE	9.50 / 98.02	11.90 / 97.63	28.18 / 93.95	36.18 / 91.96	21.44 / 95.39
BFAct	15.94 / 96.47	28.43 / 92.87	32.66 / 91.90	40.83 / 90.79	29.46 / 93.01
LTS	10.24 / 97.87	13.06 / 97.42	27.81 / 94.01	37.68 / 91.65	22.20 / 95.24
OptFS	15.88 / 96.65	16.60 / 96.10	29.94 / 92.53	40.24 / 90.20	25.66 / 93.87
AdaSCALE-A	7.61 / 98.31	<u>10.57 / 97.88</u>	<u>20.67 / 95.62</u>	32.60 / 92.74	17.86 / 96.14
AdaSCALE-L	<u>7.78 / 98.29</u>	10.33 / 97.92	20.61 / 95.62	<u>32.97 / 92.63</u>	<u>17.92 / 96.12</u>

Table 26. Far-OOD detection results (FPR@95↓ / AUROC↑) on ImageNet-1k benchmark using ResNet-50 network. The best results are **bold**, and the second-best results are underlined.

Method	iNaturalist	Textures	OpenImage-O	Places	Average
MSP	48.30 / 86.27	59.00 / 83.60	49.36 / 84.82	58.84 / 80.56	53.87 / 83.81
MLS	41.11 / 88.83	43.59 / 89.85	38.13 / 89.25	52.74 / 85.28	43.89 / 88.30
EBO	41.65 / 88.30	43.66 / 90.14	38.48 / 89.12	53.42 / 85.37	44.30 / 88.23
ReAct	19.86 / 95.66	26.94 / 93.78	30.18 / 92.54	42.58 / 90.41	29.89 / 93.10
ASH	19.90 / 95.68	13.94 / 97.32	27.76 / 93.63	43.11 / 89.59	26.18 / 94.06
SCALE	13.90 / 97.05	<u>9.34 / 98.04</u>	25.91 / 94.47	40.99 / 90.64	22.54 / 95.05
BFAct	19.60 / 95.69	25.79 / 93.79	30.18 / 92.55	42.14 / 90.13	29.43 / 93.04
LTS	15.07 / 96.83	10.33 / 97.89	25.51 / 94.52	41.40 / 90.53	23.07 / 94.94
OptFS	19.11 / 95.70	16.53 / 96.35	28.76 / 92.94	43.47 / 89.22	26.97 / 93.55
AdaSCALE-A	10.74 / 97.64	8.90 / 98.21	<u>18.75 / 96.03</u>	35.66 / 91.92	18.51 / 95.95
AdaSCALE-L	<u>11.71 / 97.36</u>	10.44 / 97.93	17.87 / 96.18	<u>36.57 / 91.55</u>	<u>19.15 / 95.76</u>

Table 27. Far-OOD detection results (FPR@95↓ / AUROC↑) on ImageNet-1k benchmark using ResNet-101 network. The best results are **bold**, and the second-best results are underlined.

Method	iNaturalist	Textures	OpenImage-O	Places	Average
MSP	28.13 / 94.67	44.73 / 88.48	36.27 / 91.96	52.51 / 85.21	40.41 / 90.08
MLS	9.10 / 98.05	39.74 / 92.82	25.71 / 95.70	57.14 / 88.22	32.92 / 93.70
EBO	7.72 / 98.29	38.18 / 93.02	25.94 / 95.83	58.04 / 88.13	32.47 / 93.82
ReAct	21.24 / 94.14	41.20 / 87.25	43.46 / 89.20	74.92 / 74.10	45.20 / 86.17
ASH	48.89 / 87.39	45.75 / 88.79	70.98 / 82.52	72.99 / 77.06	59.65 / 83.94
SCALE	11.13 / 97.88	28.29 / 95.31	33.59 / 94.87	55.62 / 88.59	32.16 / 94.16
BFAct	37.88 / 86.24	54.87 / 77.64	62.53 / 79.59	79.46 / 65.39	58.69 / 77.22
LTS	14.29 / 97.52	<u>25.21 / 95.72</u>	43.38 / 93.53	57.08 / 87.51	34.99 / 93.57
OptFS	28.95 / 93.68	39.99 / 90.13	44.96 / 89.85	75.59 / 73.24	47.37 / 86.73
AdaSCALE-A	4.34 / 99.09	26.06 / 95.21	13.09 / 97.57	41.98 / 91.48	<u>21.37 / 95.84</u>
AdaSCALE-L	<u>4.41 / 99.02</u>	13.50 / 97.61	<u>18.56 / 96.92</u>	<u>43.93 / 91.22</u>	20.10 / 96.19

Table 28. Far-OOD detection results (FPR@95↓ / AUROC↑) on ImageNet-1k benchmark using RegNet-Y-16 network. The best results are **bold**, and the second-best results are underlined.

Method	iNaturalist	Textures	OpenImage-O	Places	Average
MSP	43.56 / 88.04	62.23 / 82.13	48.06 / 85.65	58.42 / 81.02	53.07 / 84.21
MLS	32.96 / 90.93	51.58 / 87.39	37.33 / 89.80	57.76 / 83.77	44.91 / 87.97
EBO	33.42 / 90.54	51.73 / 87.56	37.79 / 89.72	57.56 / 83.62	45.12 / 87.86
ReAct	17.64 / 95.95	32.86 / 91.67	29.82 / 92.37	39.92 / 90.76	30.06 / 92.69
ASH	17.90 / 96.22	23.74 / 95.18	30.83 / 93.13	44.21 / 89.35	29.17 / 93.47
SCALE	15.66 / 96.75	27.75 / 94.94	31.43 / 93.41	47.62 / 89.08	30.62 / 93.54
BFAct	17.40 / 95.91	32.00 / 91.83	29.53 / 92.38	39.89 / 90.57	29.71 / 92.67
LTS	16.29 / 96.63	26.64 / 95.07	30.50 / 93.50	48.04 / 88.78	30.37 / 93.49
OptFS	17.20 / 96.12	23.11 / 94.69	29.59 / 92.75	40.24 / 90.05	27.54 / 93.40
AdaSCALE-A	10.02 / 97.80	17.99 / 96.38	<u>22.93 / 95.17</u>	37.38 / 91.62	22.08 / 95.24
AdaSCALE-L	<u>11.28 / 97.45</u>	<u>18.46 / 96.20</u>	21.23 / 95.35	<u>37.68 / 91.03</u>	<u>22.16 / 95.01</u>

Table 29. Far-OOD detection results (FPR@95↓ / AUROC↑) on ImageNet-1k benchmark using ResNeXt-50 network. The best results are **bold**, and the second-best results are underlined.

Method	iNaturalist	Textures	OpenImage-O	Places	Average
MSP	42.02 / 89.84	62.33 / 81.56	50.31 / 85.19	59.74 / 81.14	53.60 / 84.43
MLS	31.99 / 92.11	57.75 / 85.56	42.70 / 88.28	61.30 / 83.82	48.43 / 87.44
EBO	33.12 / 91.46	57.47 / 85.55	43.75 / 87.91	61.46 / 83.67	48.95 / 87.15
ReAct	19.41 / 95.64	23.86 / 94.63	32.54 / 91.83	47.06 / <u>88.52</u>	30.72 / 92.65
ASH	21.57 / 95.47	21.42 / 95.56	41.23 / 90.19	49.80 / 87.45	33.50 / 92.17
SCALE	18.13 / 96.29	27.22 / 94.52	34.52 / 92.15	52.82 / 87.83	33.17 / 92.70
BFAct	20.64 / 95.42	21.70 / 95.17	39.76 / 89.97	<u>47.72</u> / 88.61	32.45 / 92.29
LTS	15.68 / 96.71	22.49 / 95.81	34.27 / 92.37	51.23 / 88.26	30.92 / 93.29
OptFS	25.81 / 93.92	21.75 / 95.01	38.45 / 89.67	51.66 / 85.54	34.42 / 91.04
AdaSCALE-A	17.30 / <u>96.03</u>	<u>19.42</u> / <u>96.23</u>	23.12 / <u>94.68</u>	52.20 / 85.98	<u>28.01</u> / 93.23
AdaSCALE-L	<u>17.97</u> / 95.87	16.87 / 96.69	<u>23.64</u> / 94.69	53.50 / 85.46	28.00 / <u>93.18</u>

Table 30. Far-OOD detection results (FPR@95↓ / AUROC↑) on ImageNet-1k benchmark using DenseNet-201 network. The best results are **bold**, and the second-best results are underlined.

Method	iNaturalist	Textures	OpenImage-O	Places	Average
MSP	<u>25.14</u> / <u>95.12</u>	74.42 / 84.20	40.64 / 91.74	78.74 / 80.61	54.74 / 87.92
MLS	35.28 / 94.13	86.65 / 80.26	62.11 / 90.26	90.53 / 74.56	68.64 / 84.80
EBO	49.84 / 91.21	87.72 / 75.77	68.77 / 87.66	91.60 / 69.89	74.48 / 81.13
ReAct	46.44 / 80.96	54.56 / 77.17	60.79 / 78.20	78.39 / 64.99	60.05 / 75.33
ASH	96.26 / 37.76	95.40 / 50.98	97.52 / 43.19	97.07 / 34.34	96.56 / 41.57
SCALE	87.08 / 67.69	86.22 / 67.44	91.05 / 67.21	94.18 / 47.99	89.63 / 62.58
BFAct	57.31 / 69.11	63.43 / 67.70	69.30 / 67.49	76.86 / 58.52	66.72 / 65.70
LTS	79.05 / 84.72	86.89 / 75.39	88.00 / 81.53	93.45 / 63.56	86.85 / 76.30
OptFS	38.62 / 89.80	45.77 / 86.94	53.77 / 85.49	76.31 / 72.23	53.62 / 83.62
AdaSCALE-A	18.51 / 96.67	<u>42.07</u> / <u>90.56</u>	31.00 / 94.44	<u>58.87</u> / 84.26	37.61 / 91.48
AdaSCALE-L	26.58 / 95.02	32.81 / 92.38	<u>39.19</u> / <u>92.31</u>	56.66 / <u>82.33</u>	<u>38.81</u> / <u>90.51</u>

Table 31. Far-OOD detection results (FPR@95↓ / AUROC↑) on ImageNet-1k benchmark using EfficientNetV2-L network. The best results are **bold**, and the second-best results are underlined.

Method	iNaturalist	Textures	OpenImage-O	Places	Average
MSP	42.40 / 88.19	56.46 / 85.06	56.19 / 84.86	70.59 / 80.38	56.41 / 84.62
MLS	72.98 / 85.29	78.93 / 83.74	85.78 / 81.60	89.88 / 75.05	81.89 / 81.42
EBO	83.56 / 79.30	83.66 / 81.17	88.82 / 76.48	91.77 / 68.42	86.95 / 76.34
ReAct	48.22 / 86.11	55.87 / 86.66	57.68 / 84.29	75.48 / 77.52	59.31 / 83.65
ASH	97.02 / 50.62	98.50 / 48.53	94.79 / 55.51	93.60 / 53.97	95.98 / 52.16
SCALE	86.60 / 73.94	84.70 / 79.00	89.48 / 72.72	92.67 / 63.60	88.36 / 72.32
BFAct	40.56 / 87.96	48.65 / 88.31	48.24 / 86.59	68.86 / 80.21	51.58 / 85.77
LTS	50.42 / 88.92	61.70 / 86.53	69.26 / 83.45	76.07 / 78.82	64.37 / 84.43
OptFS	34.39 / 89.99	46.41 / 88.48	42.20 / 88.23	61.44 / 82.69	46.11 / 87.35
AdaSCALE-A	36.38 / 89.60	51.13 / 87.16	43.02 / 88.07	59.97 / 82.48	47.63 / 86.83
AdaSCALE-L	<u>35.16</u> / <u>89.84</u>	<u>50.91</u> / <u>87.37</u>	<u>43.01</u> / <u>88.13</u>	<u>60.05</u> / <u>82.55</u>	<u>47.28</u> / <u>86.97</u>

Table 32. Far-OOD detection results (FPR@95↓ / AUROC↑) on ImageNet-1k benchmark using Vit-B-16 network. The best results are **bold**, and the second-best results are underlined.

Method	iNaturalist	Textures	OpenImage-O	Places	Average
MSP	55.63 / 86.47	79.28 / 80.12	81.22 / 81.72	77.41 / 79.78	73.39 / 82.02
MLS	93.46 / 78.87	94.60 / 74.73	97.61 / 70.72	94.97 / 69.17	95.16 / 73.37
EBO	95.11 / 67.72	95.36 / 69.69	97.97 / 60.19	95.87 / 58.35	96.08 / 63.99
ReAct	40.77 / 88.60	62.26 / 85.54	58.19 / 85.76	74.21 / 79.16	58.86 / 84.77
ASH	98.59 / 42.18	98.55 / 43.37	98.23 / 43.28	97.57 / 43.98	98.23 / 43.20
SCALE	87.83 / 62.98	87.71 / 69.63	88.75 / 66.63	82.08 / 67.82	86.59 / 66.77
BFAct	25.76 / <u>91.42</u>	45.73 / 87.34	32.13 / 91.02	52.33 / 84.08	38.99 / 88.47
LTS	57.92 / 86.10	77.66 / 78.02	73.20 / 80.16	82.69 / 72.71	72.86 / 79.25
OptFS	31.94 / 90.56	<u>50.27</u> / <u>86.91</u>	<u>36.50</u> / <u>90.18</u>	58.38 / 83.51	<u>44.27</u> / 87.79
AdaSCALE-A	32.82 / 90.73	61.82 / 85.34	38.58 / 89.78	58.02 / 82.71	47.81 / 87.14
AdaSCALE-L	<u>30.95</u> / 91.69	60.17 / 86.30	37.52 / 90.08	<u>56.32</u> / <u>83.82</u>	46.24 / <u>87.97</u>

Table 33. Far-OOD detection results (FPR@95↓ / AUROC↑) on ImageNet-1k benchmark using Swin-B network. The best results are **bold**, and the second-best results are underlined.

E.3. Full-Spectrum near-OOD detection

Method	SSB-Hard	NINCO	ImageNet-O	Average
MSP	88.17 / 47.34	78.15 / 54.73	96.29 / 13.81	87.54 / 38.63
MLS	90.04 / 43.32	82.06 / 50.23	95.59 / 18.94	89.23 / 37.50
EBO	90.19 / 42.62	82.64 / 49.01	95.54 / 19.57	89.46 / 37.07
ReAct	90.65 / 45.19	80.05 / 53.37	93.62 / 26.15	88.10 / 41.57
ASH	88.82 / 44.08	78.35 / 54.54	92.48 / 30.49	86.55 / 43.04
SCALE	85.85 / 48.10	77.54 / 57.01	93.26 / 32.58	85.55 / 45.90
BFAct	90.43 / 45.29	79.62 / 53.50	93.62 / 26.20	87.89 / 41.66
LTS	86.37 / 47.43	77.54 / 56.40	93.61 / 30.57	85.84 / 44.80
OptFS	90.78 / 44.01	77.24 / 54.91	90.91 / 32.26	86.31 / 43.73
AdaSCALE-A	81.30 / 51.88	74.13 / 58.55	89.15 / 37.62	81.52 / 49.35
AdaSCALE-L	<u>81.85 / 51.38</u>	<u>74.42 / 58.23</u>	<u>90.07 / 36.91</u>	<u>82.11 / 48.84</u>

Table 34. Near-FSOOD detection results (FPR@95↓ / AUROC↑) on ImageNet-1k benchmark using ResNet-50 network. The best results are **bold**, and the second-best results are underlined.

Method	SSB-Hard	NINCO	ImageNet-O	Average
MSP	87.09 / 49.18	76.45 / 56.92	94.24 / 28.33	85.93 / 44.81
MLS	88.90 / 46.45	79.19 / 53.62	93.94 / 31.76	87.34 / 43.94
EBO	89.02 / 45.99	79.60 / 52.66	93.87 / 32.40	87.50 / 43.68
ReAct	89.50 / 47.79	77.22 / 56.02	89.37 / 39.62	85.36 / 47.81
ASH	87.84 / 46.39	75.36 / 56.72	88.48 / 42.80	83.90 / 48.64
SCALE	85.81 / 48.94	75.33 / <u>58.79</u>	88.49 / 44.45	83.21 / 50.73
BFAct	89.19 / 48.07	76.94 / 56.02	89.54 / 39.65	85.22 / 47.91
LTS	86.02 / 48.72	<u>74.89</u> / 58.41	89.17 / 43.02	83.36 / 50.05
OptFS	89.63 / 46.23	75.52 / 56.71	85.82 / 44.21	83.65 / 49.05
AdaSCALE-A	82.33 / 51.47	74.38 / 59.17	<u>82.89 / 48.49</u>	79.87 / 53.04
AdaSCALE-L	<u>82.53 / 51.31</u>	75.22 / 58.62	82.19 / 48.03	<u>79.98 / 52.66</u>

Table 35. Near-FSOOD detection results (FPR@95↓ / AUROC↑) on ImageNet-1k benchmark using ResNet-101 network. The best results are **bold**, and the second-best results are underlined.

Method	SSB-Hard	NINCO	ImageNet-O	Average
MSP	83.74 / 57.23	72.32 / 67.69	87.81 / 56.61	81.29 / 60.51
MLS	82.91 / 60.89	71.22 / 70.86	93.27 / 55.21	82.46 / 62.32
EBO	<u>82.77</u> / 61.63	<u>71.17</u> / <u>71.23</u>	93.39 / 55.02	82.44 / 62.63
ReAct	87.74 / 55.64	80.22 / 65.24	91.11 / 55.13	86.36 / 58.67
ASH	87.26 / 57.45	84.81 / 61.59	93.78 / 54.76	88.61 / 57.93
SCALE	83.23 / <u>61.02</u>	72.48 / 71.33	92.82 / 57.16	82.84 / 63.17
BFAct	90.46 / 54.73	87.03 / 61.98	92.37 / 54.13	89.96 / 56.95
LTS	83.53 / 60.77	74.23 / 70.84	92.30 / 57.71	83.35 / 63.11
OptFS	90.33 / 51.78	80.82 / 63.86	88.86 / 59.45	86.67 / 58.36
AdaSCALE-A	81.68 / 60.46	68.05 / 70.95	<u>83.25</u> / <u>60.91</u>	77.66 / 64.11
AdaSCALE-L	84.30 / 59.42	76.30 / 68.49	81.86 / 63.12	<u>80.82</u> / <u>63.68</u>

Table 36. Near-FSOOD detection results (FPR@95↓ / AUROC↑) on ImageNet-1k benchmark using RegNet-Y-16 network. The best results are **bold**, and the second-best results are underlined.

Method	SSB-Hard	NINCO	ImageNet-O	Average
MSP	86.95 / 49.77	78.27 / 57.25	94.79 / 28.95	86.67 / 45.32
MLS	88.56 / 47.94	81.58 / 54.31	94.26 / 32.40	88.13 / 44.88
EBO	88.68 / 47.69	81.67 / 53.51	94.21 / 32.99	88.19 / 44.73
ReAct	89.45 / 47.44	80.37 / 55.29	91.40 / 37.58	87.07 / 46.77
ASH	86.26 / 49.73	79.62 / 57.17	92.63 / 39.67	86.17 / 48.86
SCALE	84.64 / 52.60	78.75 / <u>58.90</u>	94.20 / 37.99	85.86 / 49.83
BFAct	89.22 / 47.70	80.39 / 55.34	91.24 / 37.66	86.95 / 46.90
LTS	85.03 / 51.87	78.65 / 58.48	93.77 / 37.96	85.82 / 49.43
OptFS	89.63 / 46.23	<u>75.52</u> / 56.71	<u>85.82</u> / <u>44.21</u>	83.65 / 49.05
AdaSCALE-A	82.33 / 51.47	74.38 / 59.17	82.89 / 48.49	79.87 / 53.04
AdaSCALE-L	<u>82.70</u> / <u>52.14</u>	75.85 / 58.05	89.55 / 43.81	<u>82.70</u> / <u>51.33</u>

Table 37. Near-FSOOD detection results (FPR@95↓ / AUROC↑) on ImageNet-1k benchmark using ResNeXt-50 network. The best results are **bold**, and the second-best results are underlined.

Method	SSB-Hard	NINCO	ImageNet-O	Average
MSP	87.27 / 49.71	76.81 / 58.30	95.00 / 29.36	86.36 / 45.79
MLS	89.24 / 47.21	80.48 / 55.21	95.61 / 30.74	88.44 / 44.39
EBO	89.39 / 46.79	80.94 / 54.13	95.60 / 31.44	88.65 / 44.12
ReAct	90.76 / 45.54	79.54 / 55.57	88.40 / 42.63	86.23 / 47.91
ASH	89.75 / 47.08	81.35 / 58.13	90.47 / 46.81	87.19 / 50.67
SCALE	87.55 / 49.53	78.35 / 59.54	92.79 / 39.22	86.23 / 49.43
BFAct	92.33 / 44.88	83.90 / 54.83	84.88 / 49.50	87.04 / 49.74
LTS	87.30 / 50.02	<u>78.41</u> / 60.35	92.12 / 42.25	85.94 / <u>50.88</u>
OptFS	92.32 / 43.61	81.45 / 56.09	85.02 / 50.48	86.26 / 50.06
AdaSCALE-A	86.22 / 48.41	80.25 / 56.38	<u>81.35</u> / 47.45	82.60 / 50.75
AdaSCALE-L	<u>86.43</u> / <u>48.54</u>	80.83 / 56.30	81.00 / <u>50.00</u>	<u>82.75</u> / 51.61

Table 38. Near-FSOOD detection results (FPR@95↓ / AUROC↑) on ImageNet-1k benchmark using DenseNet-201 network. The best results are **bold**, and the second-best results are underlined.

Method	SSB-Hard	NINCO	ImageNet-O	Average
MSP	83.74 / 57.23	72.32 / 67.69	87.81 / 56.61	81.29 / 60.51
MLS	82.91 / 60.89	71.22 / 70.86	93.27 / 55.21	82.46 / 62.32
EBO	82.77 / 61.63	71.17 / 71.23	93.39 / 55.02	82.44 / 62.63
ReAct	87.74 / 55.64	80.22 / 65.24	91.11 / 55.13	86.36 / 58.67
ASH	87.26 / 57.45	84.81 / 61.59	93.78 / 54.76	88.61 / 57.93
SCALE	<u>83.23</u> / <u>61.02</u>	72.48 / 71.33	92.82 / 57.16	82.84 / 63.17
BFAct	90.46 / 54.73	87.03 / 61.98	92.37 / 54.13	89.96 / 56.95
LTS	83.53 / 60.77	74.23 / <u>70.84</u>	92.30 / 57.71	83.35 / 63.11
OptFS	90.33 / 51.78	80.82 / 63.86	88.86 / 59.45	86.67 / 58.36
AdaSCALE-A	81.68 / 60.46	68.05 / 70.95	<u>83.25</u> / <u>60.91</u>	77.66 / 64.11
AdaSCALE-L	84.30 / 59.42	76.30 / 68.49	81.86 / 63.12	<u>80.82</u> / <u>63.68</u>

Table 39. Near-FSOOD detection results (FPR@95↓ / AUROC↑) on ImageNet-1k benchmark using EfficientNetV2-L network. The best results are **bold**, and the second-best results are underlined.

Method	SSB-Hard	NINCO	ImageNet-O	Average
MSP	<u>92.28</u> / <u>47.57</u>	87.44 / 56.23	98.02 / 39.33	92.58 / 47.71
MLS	94.11 / 44.88	95.17 / 52.44	98.00 / 37.77	95.76 / 45.03
EBO	94.47 / 42.06	95.86 / 48.45	97.89 / 38.03	96.07 / 42.85
ReAct	94.95 / 41.84	88.65 / 52.48	95.21 / 44.64	92.94 / 46.32
ASH	88.95 / 56.47	91.09 / 55.11	90.00 / 55.78	90.01 / 55.79
SCALE	94.52 / 41.21	96.30 / 45.78	97.76 / 37.09	96.19 / 41.36
BFAct	94.99 / 41.44	85.62 / 53.35	92.62 / 45.64	91.07 / 46.81
LTS	95.33 / 43.36	90.52 / 53.14	95.90 / 41.30	93.91 / 45.93
OptFS	94.19 / 43.01	81.66 / <u>55.60</u>	88.90 / <u>46.04</u>	88.25 / 48.22
AdaSCALE-A	93.30 / 42.49	<u>81.00</u> / 54.72	84.12 / 45.71	86.14 / <u>47.64</u>
AdaSCALE-L	93.52 / 41.83	80.94 / 54.16	<u>84.26</u> / 45.82	<u>86.24</u> / 47.27

Table 40. Near-FSOOD detection results (FPR@95↓ / AUROC↑) on ImageNet-1k benchmark using ViT-B-16 network. The best results are **bold**, and the second-best results are underlined.

Method	SSB-Hard	NINCO	ImageNet-O	Average
MSP	91.55 / 53.29	86.73 / 60.62	97.85 / 42.90	92.04 / 52.27
MLS	94.49 / 50.01	93.94 / 56.40	97.11 / 43.76	95.18 / 50.06
EBO	94.66 / 47.41	94.58 / 52.04	96.76 / 45.84	95.33 / 48.43
ReAct	94.04 / 47.83	82.85 / 58.52	94.60 / 50.41	90.50 / 52.25
ASH	91.77 / <u>50.35</u>	90.91 / 52.09	88.80 / <u>54.50</u>	90.49 / 52.31
SCALE	93.39 / 47.38	91.25 / 53.00	90.80 / 56.10	91.81 / 52.16
BFAct	92.65 / 48.33	79.61 / <u>59.66</u>	84.26 / 53.17	85.51 / 53.72
LTS	94.26 / 48.70	88.32 / 57.60	93.04 / 46.33	91.87 / 50.88
OptFS	94.06 / 47.77	81.91 / 59.14	<u>86.95</u> / 51.34	87.64 / <u>52.75</u>
AdaSCALE-A	<u>90.29</u> / 46.84	81.54 / 57.44	87.74 / 47.55	86.52 / 50.61
AdaSCALE-L	90.18 / 46.63	<u>80.77</u> / 57.85	87.27 / 47.90	<u>86.07</u> / 50.79

Table 41. Near-FSOOD detection results (FPR@95↓ / AUROC↑) on ImageNet-1k benchmark using Swin-B network. The best results are **bold**, and the second-best results are underlined.

E.4. Full-Spectrum far-OOD detection

Method	iNaturalist	Textures	OpenImage-O	Places	Average
MSP	69.31 / 65.65	80.57 / 59.22	73.94 / 60.74	79.02 / 56.04	75.71 / 60.41
MLS	64.71 / 63.30	74.69 / 61.67	69.73 / 60.60	80.04 / 55.08	72.29 / 60.16
EBO	65.30 / 61.43	74.48 / 61.87	69.92 / 59.93	80.12 / 54.48	72.45 / 59.42
ReAct	51.90 / 75.79	63.55 / 69.22	65.64 / 67.36	71.81 / 67.01	63.22 / 69.84
ASH	49.21 / 76.93	50.54 / 77.64	63.04 / 69.03	70.62 / 64.79	58.35 / 72.10
SCALE	43.34 / 79.23	46.60 / 79.58	62.26 / 70.54	67.94 / 67.05	55.04 / 74.10
BFAct	51.01 / 75.85	62.45 / 69.03	65.52 / 67.21	71.17 / 66.45	62.54 / 69.63
LTS	45.12 / 78.72	48.77 / 79.13	62.43 / 70.17	69.31 / 66.20	56.41 / 73.55
OptFS	49.39 / 77.14	50.25 / 75.59	62.46 / 68.87	69.84 / 65.65	57.99 / 71.81
AdaSCALE-A	41.24 / 79.53	45.55 / <u>79.64</u>	56.43 / 72.85	66.13 / 67.54	52.33 / 74.89
AdaSCALE-L	<u>41.75</u> / 79.63	<u>45.67</u> / 79.96	<u>56.80</u> / <u>72.82</u>	<u>66.69</u> / <u>67.28</u>	<u>52.73</u> / <u>74.92</u>

Table 42. Far-FSOOD detection results (FPR@95↓ / AUROC↑) on ImageNet-1k benchmark using ResNet-50 network. The best results are **bold**, and the second-best results are underlined.

Method	iNaturalist	Textures	OpenImage-O	Places	Average
MSP	71.78 / 64.51	78.82 / 62.20	72.52 / 62.27	78.71 / 57.55	75.46 / 61.63
MLS	70.55 / 62.07	72.11 / 65.46	68.68 / 62.27	77.60 / 58.03	72.23 / 61.96
EBO	70.94 / 60.64	72.18 / 65.71	68.96 / 61.59	77.97 / 57.75	72.51 / 61.42
ReAct	53.59 / 75.05	59.92 / 72.13	62.45 / 69.16	71.14 / 66.87	61.78 / 70.80
ASH	53.84 / 74.07	47.67 / 79.09	60.66 / 70.12	71.45 / 64.40	58.40 / 71.92
SCALE	47.82 / 76.79	42.04 / 80.95	59.26 / 71.76	70.32 / 65.86	54.86 / 73.84
BFAct	53.23 / 74.86	58.84 / 71.86	62.33 / 68.97	70.67 / 66.17	61.27 / 70.47
LTS	49.64 / 76.17	43.87 / 80.60	59.32 / 71.46	70.85 / 65.35	55.92 / 73.39
OptFS	51.52 / 75.52	48.88 / 76.96	59.99 / 70.28	70.86 / 65.15	57.81 / 71.98
AdaSCALE-A	44.77 / 77.51	42.17 / 80.73	<u>53.58</u> / 73.90	67.14 / 66.84	51.91 / 74.75
AdaSCALE-L	<u>46.52</u> / <u>76.39</u>	<u>44.87</u> / <u>79.90</u>	53.32 / <u>73.81</u>	<u>68.16</u> / <u>65.88</u>	<u>53.22</u> / <u>73.99</u>

Table 43. Far-FSOOD detection results (FPR@95↓ / AUROC↑) on ImageNet-1k benchmark using ResNet-101 network. The best results are **bold**, and the second-best results are underlined.

Method	iNaturalist	Textures	OpenImage-O	Places	Average
MSP	53.98 / 80.49	69.36 / 70.97	62.02 / 75.95	75.48 / 65.76	65.21 / 73.29
MLS	39.99 / 85.09	69.12 / 73.89	58.30 / 80.08	79.98 / 66.96	61.85 / 76.51
EBO	38.42 / 86.11	68.23 / 74.16	58.77 / 80.93	80.56 / 67.08	61.49 / 77.07
ReAct	43.95 / 85.15	66.24 / 73.34	68.23 / 77.80	88.79 / 57.47	66.80 / 73.44
ASH	61.03 / 79.08	58.16 / 80.78	80.03 / 74.57	81.60 / 67.74	70.21 / 75.54
SCALE	39.13 / 86.34	56.30 / 79.93	60.66 / 81.10	76.25 / 70.04	58.09 / 79.35
BFAct	52.17 / 82.68	71.55 / 70.74	78.37 / 74.00	90.50 / 56.09	73.15 / 70.88
LTS	38.98 / 86.90	50.10 / 82.26	65.29 / 81.17	75.41 / 70.91	57.44 / 80.31
OptFS	52.61 / 82.40	<u>62.47</u> / <u>76.57</u>	66.68 / 76.79	88.01 / 56.14	67.44 / 72.98
AdaSCALE-A	<u>34.25</u> / <u>87.68</u>	63.81 / 76.12	50.37 / <u>82.13</u>	<u>74.81</u> / 68.37	<u>55.81</u> / 78.58
AdaSCALE-L	32.72 / 88.82	47.93 / 82.84	<u>53.84</u> / 83.09	73.90 / <u>70.37</u>	52.10 / 81.28

Table 44. Far-FSOD detection results (FPR@95 \downarrow / AUROC \uparrow) on ImageNet-1k benchmark using RegNet-Y-16 network. The best results are **bold**, and the second-best results are underlined.

Method	iNaturalist	Textures	OpenImage-O	Places	Average
MSP	68.90 / 66.67	80.91 / 60.21	71.91 / 63.25	78.58 / 57.84	75.07 / 62.00
MLS	64.59 / 65.49	76.51 / 62.51	67.70 / 63.96	79.89 / 56.90	72.17 / 62.21
EBO	64.95 / 64.23	76.59 / 62.61	68.00 / 63.52	79.80 / 56.39	72.34 / 61.69
ReAct	51.97 / 76.08	65.34 / 68.27	63.05 / 68.94	70.13 / 67.58	62.62 / 70.22
ASH	53.84 / 74.07	<u>47.67</u> / 79.09	60.66 / 70.12	71.45 / 64.40	58.40 / 71.92
SCALE	49.27 / <u>76.82</u>	60.07 / 75.14	62.91 / 70.69	73.38 / 64.22	61.41 / 71.72
BFAct	53.23 / 74.86	58.84 / 71.86	62.33 / 68.97	70.67 / 66.17	61.27 / 70.47
LTS	49.64 / 76.17	48.77 / <u>79.13</u>	62.43 / 70.17	70.85 / 65.35	<u>56.41</u> / <u>73.55</u>
OptFS	51.52 / 75.77	50.25 / 75.59	62.46 / 68.87	69.84 / 65.65	57.99 / 71.81
AdaSCALE-A	43.82 / 78.47	45.55 / 79.64	56.43 / 72.85	66.13 / <u>67.54</u>	52.33 / 74.89
AdaSCALE-L	<u>46.23</u> / 76.67	54.29 / 75.80	<u>56.84</u> / <u>72.44</u>	<u>69.13</u> / 64.99	56.62 / 72.47

Table 45. Far-FSOD detection results (FPR@95 \downarrow / AUROC \uparrow) on ImageNet-1k benchmark using ResNeXt-50 network. The best results are **bold**, and the second-best results are underlined.

Method	iNaturalist	Textures	OpenImage-O	Places	Average
MSP	68.90 / 66.67	80.91 / 60.21	71.91 / 63.25	78.58 / 57.84	75.07 / 62.00
MLS	64.59 / 65.49	76.51 / 62.51	67.70 / 63.96	79.89 / 56.90	72.17 / 62.21
EBO	64.95 / 64.23	76.59 / 62.61	68.00 / 63.52	79.80 / 56.39	72.34 / 61.69
ReAct	51.97 / 76.08	65.34 / 68.27	63.05 / 68.94	<u>70.13</u> / 67.58	62.62 / 70.22
ASH	53.84 / 74.07	47.67 / <u>79.09</u>	60.66 / 70.12	71.45 / 64.40	58.40 / 71.92
SCALE	49.27 / 76.82	60.07 / 75.14	62.91 / 70.69	73.38 / 64.22	61.41 / 71.72
BFAct	53.23 / 74.86	58.84 / 71.86	62.33 / 68.97	70.67 / <u>66.17</u>	61.27 / 70.47
LTS	49.64 / <u>76.17</u>	<u>48.77</u> / 79.13	62.43 / 70.17	70.85 / 65.35	56.41 / 73.55
OptFS	51.52 / 75.77	50.25 / 75.59	62.46 / 68.87	69.84 / 65.65	<u>57.99</u> / <u>71.81</u>
AdaSCALE-A	52.55 / 73.62	54.70 / 76.19	58.11 / <u>71.31</u>	77.77 / 58.83	60.78 / 69.99
AdaSCALE-L	53.04 / 73.62	51.83 / 78.00	<u>58.30</u> / 71.92	78.40 / 58.47	60.39 / 70.50

Table 46. Far-FSOD detection results (FPR@95↓ / AUROC↑) on ImageNet-1k benchmark using DenseNet-201 network. The best results are **bold**, and the second-best results are underlined.

Method	iNaturalist	Textures	OpenImage-O	Places	Average
MSP	53.98 / 80.49	69.36 / 70.97	62.02 / 75.95	75.48 / 65.76	65.21 / 73.29
MLS	39.99 / 85.09	69.12 / 73.89	58.30 / 80.08	79.98 / 66.96	61.85 / 76.51
EBO	38.42 / 86.11	68.23 / 74.16	58.77 / 80.93	80.56 / 67.08	61.49 / 77.07
ReAct	43.95 / 85.15	66.24 / 73.34	68.23 / 77.80	88.79 / 57.47	66.80 / 73.44
ASH	61.03 / 79.08	58.16 / 80.78	80.03 / 74.57	81.60 / 67.74	70.21 / 75.54
SCALE	39.13 / 86.34	56.30 / 79.93	60.66 / 81.10	76.25 / 70.04	58.09 / 79.35
BFAct	52.17 / 82.68	71.55 / 70.74	78.37 / 74.00	90.50 / 56.09	73.15 / 70.88
LTS	<u>38.98</u> / 86.90	<u>50.10</u> / <u>82.26</u>	65.29 / 81.17	<u>75.41</u> / 70.91	<u>57.44</u> / <u>80.31</u>
OptFS	52.61 / 82.40	62.47 / 76.57	66.68 / 76.79	88.01 / 56.14	67.44 / 72.98
AdaSCALE-A	40.76 / 88.62	63.95 / 77.69	53.96 / 84.71	77.17 / 69.22	58.96 / 80.06
AdaSCALE-L	43.28 / <u>87.91</u>	<u>50.23</u> / 83.05	<u>57.11</u> / <u>84.45</u>	73.87 / <u>70.29</u>	56.12 / 81.43

Table 47. Far-FSOD detection results (FPR@95↓ / AUROC↑) on ImageNet-1k benchmark using EfficientNetV2-L network. The best results are **bold**, and the second-best results are underlined.

Method	iNaturalist	Textures	OpenImage-O	Places	Average
MSP	66.12 / 67.29	75.49 / 64.02	75.32 / 63.46	83.84 / 58.77	75.19 / 63.39
MLS	82.34 / 64.58	85.83 / 63.52	90.12 / 61.11	92.95 / 55.08	87.81 / 61.07
EBO	87.94 / 59.51	88.03 / 62.20	91.84 / 57.54	94.14 / 50.68	90.49 / 57.48
ReAct	70.31 / 62.56	75.49 / 64.90	76.64 / 61.30	87.02 / 54.77	77.37 / 60.88
ASH	93.23 / 53.23	95.19 / 51.16	90.38 / 57.95	89.04 / 56.56	91.96 / 54.72
SCALE	90.13 / 55.74	88.71 / 61.09	92.30 / 55.21	94.75 / 47.62	91.47 / 54.92
BFAct	66.39 / 62.89	71.84 / <u>65.55</u>	<u>71.56</u> / 62.19	84.23 / 55.84	73.51 / 61.62
LTS	71.01 / <u>67.15</u>	78.15 / 65.01	82.72 / 60.98	86.73 / 56.56	79.65 / 62.43
OptFS	62.89 / 66.41	70.96 / 65.68	68.25 / 64.30	80.02 / <u>58.53</u>	70.53 / 63.73
AdaSCALE-A	<u>65.49</u> / 65.27	74.75 / 63.69	<u>69.79</u> / 63.49	79.93 / 57.47	72.49 / <u>62.48</u>
AdaSCALE-L	64.72 / 64.84	74.72 / 63.49	69.92 / 62.86	79.99 / 57.04	<u>72.34</u> / 62.06

Table 48. Far-FSOD detection results (FPR@95↓ / AUROC↑) on ImageNet-1k benchmark using ViT-B-16 network. The best results are **bold**, and the second-best results are underlined.

Method	iNaturalist	Textures	OpenImage-O	Places	Average
MSP	73.78 / 70.69	87.48 / 63.62	88.58 / 65.05	86.43 / 62.22	84.07 / 65.39
MLS	94.01 / 64.59	94.98 / 61.02	97.72 / 57.01	95.29 / 54.55	95.50 / 59.29
EBO	95.11 / 55.73	95.35 / 58.70	97.99 / 49.71	95.87 / 47.30	96.08 / 52.86
ReAct	66.17 / 68.53	79.27 / 66.85	76.92 / 65.82	85.99 / 57.89	77.09 / 64.77
ASH	94.55 / 47.18	94.43 / 48.22	93.77 / 48.28	92.55 / 48.99	93.82 / 48.17
SCALE	91.23 / 53.32	91.15 / 60.76	91.87 / 57.44	87.05 / 58.13	90.32 / 57.41
BFAct	54.53 / 73.59	69.73 / 68.65	59.76 / 74.29	74.09 / 64.30	64.53 / 70.21
LTS	72.97 / 70.44	86.21 / 62.18	83.29 / 63.87	89.39 / 56.32	82.96 / 63.20
OptFS	<u>58.91</u> / <u>71.84</u>	<u>72.14</u> / <u>68.00</u>	<u>62.45</u> / <u>72.16</u>	77.16 / <u>63.35</u>	<u>67.66</u> / <u>68.83</u>
AdaSCALE-A	61.33 / 68.58	79.90 / 64.03	65.40 / 67.52	77.68 / 59.21	71.08 / 64.83
AdaSCALE-L	60.15 / 70.58	78.72 / 65.23	64.83 / 68.17	<u>76.43</u> / 60.64	70.03 / 66.15

Table 49. Far-FSOD detection results (FPR@95↓ / AUROC↑) on ImageNet-1k benchmark using Swin-B network. The best results are **bold**, and the second-best results are underlined.